LATVIAN JOURNAL of PHYSICS and TECHNICAL SCIENCES

ISSN 0868 - 8257

6

(Vol. 57)

2020

CONTENTS

LATVIAN JOURNAL of PHYSICS and TECHNICAL SCIENCES

LATVIJAS FIZIKAS un TEHNISKO ZINĀTŅU ŽURNĀLS

ЛАТВИЙСКИЙ ФИЗИКО-ТЕХНИЧЕСКИЙ ЖУРНАЛ

Published six times a year since February 1964
Iznāk sešas reizes gadā kopš 1964. gada februāra
Выходит шесть раз в год с февраля 1964 года

6 (Vol. 57) • 2020

RĪGA

Language Editor: O. Ivanova
Computer Designer: I. Begicevs

INDEXED (PUBLISHED) IN

www.scopus.com
www.sciendo.com
EBSCO (Academic Search Complete, www.epnet.com), INSPEC (www.iee.org.com).
VINITI (www.viniti.ru), Begell House Inc/ (EDC, www.edata-center.com).

Issuers: Institute of Physical Energetics,
Institute of Solid State Physics, University of Latvia
Registration Certificate Number: 000700221

Editorial Contacts:
11 Krivu Street, Riga, LV - 1006
Ph.: + 371 67551732
E-mail: leo@lza.lv
www.fei-web.lv

sciendo

LATVIAN JOURNAL OF PHYSICS
AND TECHNICAL SCIENCES
2020, N 6

DOI: 10.2478/lpts-2020-0029

COMPUTER SIMULATION OF THE ELECTRIC TRANSPORT PROPERTIES OF THE FeSe MONOLAYER

D. Sergeyev[1,2]*, N. Zhanturina[1], L. Myasnikova[1],
A.I. Popov[3], A. Duisenova[1], A. Istlyaup[1]

[1] K. Zhubanov Aktobe Regional University,
34 Alia Moldagulova Av., Aktobe, 030000, KAZAKHSTAN
[2] T. Begeldinov Aktobe Aviation Institute,
39 Alia Moldagulova Av., Aktobe, 030000, KAZAKHSTAN
[3] Institute of Solid State Physics, University of Latvia,
8 Kengaraga Str., Riga, LV-1063, LATVIA
*E-mail: serdau@mail.ru, nzhanturina@mail.ru, popov@latnet.lv

The paper deals with the model research of electric transport characteristics of stressed and non-stressed FeSe monolayers. Transmission spectra, current-voltage characteristic (CVC) and differential conductivity spectra of two-dimensional FeSe nanostructure have been calculated within the framework of the density functional theory and non-equilibrium Green's functions (DFT + NEGF). It has been shown that the electrophysical properties depend on the geometry of the sample, the substrate, and the lattice constant. On CVC of non-stressed sample in the range from -1.2 V to -1 and from 1.2 V to 1.4 V, a region of negative differential resistance (NDR) has been observed. NDR is at both signs of the applied voltage due to the symmetry of the nanostructure. d^2I/dV^2 is used to determine the nature of the electron-phonon interaction and the features of quasiparticle tunnelling in stressed and non-stressed samples. The results obtained can be useful for calculating new elements of 2D nanoelectronics.

Keywords: *Current-voltage characteristics, FeSe monolayer, transmission spectra, 2D-nanoelectronics.*

1. INTRODUCTION

Currently, reducing the size of electronic components, which consist of the circuits of all modern chips, is becoming increasingly important [1]–[11]. For further miniaturization, it is necessary to develop new nanomaterials with controlled electrophysical properties [12]. With the discovery of graphene and other two-dimensional atomic crystals, the search for new 2D nanomaterials with unusual electrophysical properties began, as well as the development of various electronic devices based on it [13]–[15]. Various technological methods for synthesizing two-dimensional monoatomic crystals based on elements of the fourth group of the periodic table are already known: germanene [16], silicene [17], borophene [18], stanene [19], phosphorene [20], etc., as well as 2D crystals based on carbides, oxides, chlorides, nitrides, transition metal dichalcogenides, etc. [21]. Recently, intensive work has been carried out on the development of nanoelectronic devices based on 2D nanomaterials: field-effect transistors, sensors, power storage devices, solar cells, etc., so a new direction of nanoelectronics has appeared – 2D-nanoelectronics, the main idea of which is to implement elements of electronic technology using 2D-nanomaterials [22]. It opens up the possibility of producing completely new electronic devices with unusual characteristics.

At this moment, the properties of electronic nanomaterials are modelled by using various computer programs. Determining the transmission properties of nanomaterials and the areas of negative differential resistance (NDR) leads to the creation of electronic components with predefined physical properties.

In this paper, the electric transport characteristics of the FeSe monolayer are modelled and analysed in the framework of the density functional theory in combination with the method of non-equilibrium Green's functions (DFT + NEGF). The first reason of our interest has been to simulate the electric transport properties of the FeSe monolayer, whose tetragonal structure of the crystal is very simple. It is completely characterised by two lattice parameters [23]. Second, when the temperature changes, FeSe undergoes small structural changes. This change between iron atoms causes the material to exhibit directional-dependent behaviour, such as the increased electrical resistance or conductivity, only in the left-to-right or forward-to-backward direction (nematic) [24].

The discovery of superconductivity in 2D-FeSe at a critical temperature T_C~65 K was quite surprising, since in bulk 3D-FeSe the T_C value did not exceed 10 K. A possible reason for this record-breaking increase in the critical temperature of the FeSe monolayer is a sharp increase in the electron concentration due to the presence of oxygen vacancies on the surface of the $SrTiO_3$ substrate [25]. Note that paper [26] proposes an alternative approach to the deposition of potassium atoms on the surface of the FeSe monolayer to change the electron concentration. These features of the FeSe superconducting monolayer are insufficiently explained as part of the traditional phonon and spin-fluctuation mechanism of electron pairing, which requires the study of its electronic properties.

2. GEOMETRY

The geometry of the FeSe model monolayer is shown in Fig. 1 (a–b). Exploration of electric transport characteristics was carried out with samples that were not-stressed (Fig. 1a), stressed with a substrate (Fig. 1b) and without it. When a monolayer is placed on a substrate, the structure is stressed and the linear dimensions increase.

The lattice constant in the layer of the non-stressed sample is 3.765 Å, and in the layer of a stressed sample it is significantly larger and is 3.905 Å. The length of the electrodes along the C axis of the non-stressed sample is ~7.53 Å, and the stressed sample is ~7.81 Å. The length of the monolayer under examination reaches ~50.86 Å. The distance between the electrodes for a non-stressed and stressed structure is 35.8 Å and 37.14 Å, respectively.

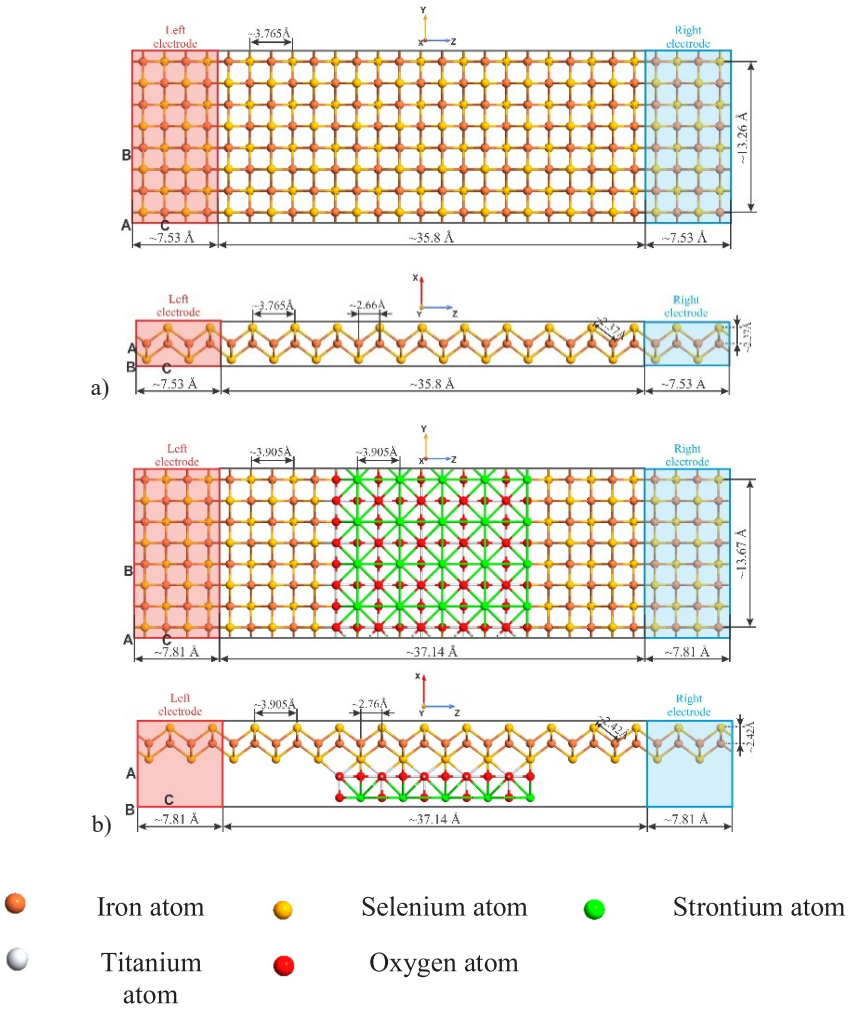

Fig. 1. The geometry of the sample.

For optimization, the 2D-FeSe geometry and description of the interaction between its atoms DFT were used with the exchange-correlation functional GGA-PBE [27], [28].

3. SIMULATION MODEL AND METHODS

Calculations of electric transport characteristics of 2D-FeSe were performed in the framework of DFT using the method of NEGF in the local density approximation (LDA) [29]. Modelling of quantum transport characteristics of a nanodevice is implemented in the Atomistix ToolKit with Virtual NanoLab [30]. The main equations of this method are described in detail in our works [31], [32]. The 2D-FeSe CVC is calculated on the basis of the well-known Landauer equation, which indicates the fundamental relationship of the electric current with the transmission spectrum [33]:

$$I\left(V_L,\ V_R,\ T_L,\ T_R\right)=\frac{2e}{h}\int_{-\infty}^{+\infty}T\left(\varepsilon\right)\left[f\left(\frac{\varepsilon-\mu_R}{k_BT_R}\right)-f\left(\frac{\varepsilon-\mu_L}{k_BT_L}\right)\right]d\varepsilon\,, \tag{1}$$

where e is the charge of the electron, h is Planck's constant, ε is energy, $T\left(\varepsilon\right)$ is function (spectrum) transmission, $f\left(\varepsilon\right)$ is the Fermi distribution function of quasiparticle energy, k_B is the Boltzmann's constant, T_R, T_L are the current temperatures and μ_R, μ_L are the electrochemical potentials of the right and left electrode.

The differential conductivity of the FeSe monolayer was obtained from the self-consistent current for a number of applied displacement and performing numerical differentiation.

4. RESULTS AND DISCUSSION

Evolution of the transmission spectrum, which increases with bias voltage of the monolayer from -2 V to 2 V, is shown in Fig. 2. The bias voltage increased in increments of 0.2 V.

The transmission ability of the FeSe nanostructure increases gradually as the bias voltage grows. The structure of the spectrum gets complicated and new ones appear, preserving the old ones (Fig. 1a). Increase in the number of peaks gives information about increasing indication in the transport of quasiparticles through the structure under consideration [34]. At bias voltages from 0.4 V and higher (Fig. 2 a), peaks are observed at -2.9 eV, -2.4 eV, -2.2 eV, -1.9 eV, -1.5 eV, -1.2 eV, -0.9 eV, 0.9 eV, 1.1 eV, 1.2 eV, 1.4 eV, 1.6 eV, 1.8 eV, 2 eV, 2.3 eV, 2.6 eV, 2.9 eV. The maximum peak occurred at energies of -1.2 eV and 1.2 eV. A dip in the transmission spectrum was observed at about 0.1 eV. It should be noted that for values from -2 V to -1 V, there is no transmission in the sample. From the transmission spectrum, we can conclude that resonant tunnelling is possible, which is explained by the low dimension of the FeSe monolayer.

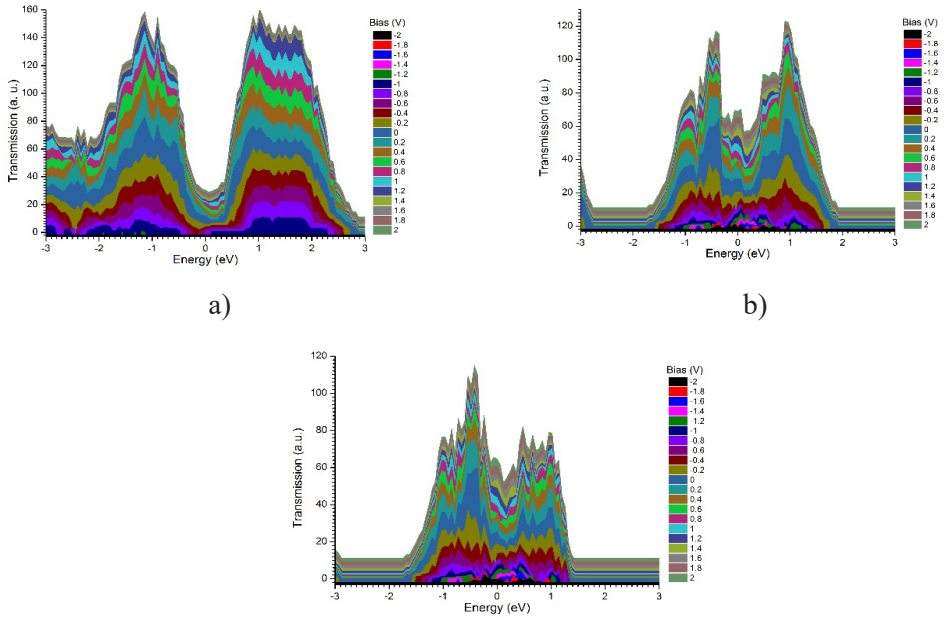

Fig. 2. Evolution of the transmission spectra of a monolayer FeSe:
a) non-stressed sample;
b) stressed sample with a substrate;
c) stressed sample without a substrate.

There are fewer peaks in a stressed sample with a substrate (Fig. 2b), which indicates lower characteristics of the electronic transport of quasiparticles. In this case, the FeSe transmission is recorded from – 2 V. The maximum transmission coefficient in this case is less than in a non-stressed sample. The electric transport characteristics are better in a sample with an increased order parameter and without a substrate, judging by the number of peaks, but the interval in which the maxima are observed is more than in a sample with a substrate.

The results of modelling the CVC and differential conductivity are shown in Fig. 3. (The CVC and differential conductivity of the nanostructures under consideration are calculated using Eqs. (1, 2)).

On CVC of the nanostructure, it can be seen that the classical traditional parameter of order in the voltage ranges from -2 V to -1.2 V, the dependence between current and voltage becomes linear and the current does not flow through the structure. A sharp drop was noted from -1.2 V to -1 V. This is a section of NDR (Fig. 3a (1) and Fig. 3b (1)). The next section of the NDR is marked in the range from 1.2 V to 1.4 V. The minimum was observed at -0.8 V. The maximum value of the non-stressed sample current was 30 μA. A section of almost linear dependence appeared in the range from 1.6 V, where the current did not flow through the FeSe monolayer. On the curves 2 and 3, negative differential resistance was not observed.

In the samples with an increased order parameter with and without Sr, Ti, O substrate, CVC was almost the same, differing only in the fact that a dip in the nanodevice

with the substrate was at -1.6 eV and CVC became N-shaped. The maximum current of 100 μA was also recorded in the sample with the substrate. In both samples, the current increased in the range from -1 V to 1 V from -100 μA to 80 μA.

In the differential conductivity spectrum in the range from -2 V to 2 V, we observed five peak structures of differential conductivity. Moreover, the intervals of NDR are characteristic only of a non-stressed film. In sample 1 (Fig. 3b) peaks were observed at -1.3 V, -0.7 V, 0 V, 1.1 V, 1.8 V. In the sample, peak structures of 10 μS, 70 μS, 90 μS, 290 μS were recorded in the region of bias voltages of -1.5 V, -0.8 V, -0.6 V, 0V, 0.5 V, 0.9 V, 1.5 V. There are a few maxima in sample 3, but they have higher differential conductivity. The maximum value of the differential conductivity in the negative side was -230 μS, in the positive 290 μS.

Minima were observed around -1.1 V, -1.7 V, 0.9 V, 1.3 V, 1.9 V. The registration of negative differential resistance at both signs of the applied voltage indicates a symmetrical structure of the FeSe molecule [34]. The value of ΔV varied from 0.2 V to 0.7 V. The nature of the resulting maxima on the differential conductivity spectrum is related to the Coulomb interaction of particles.

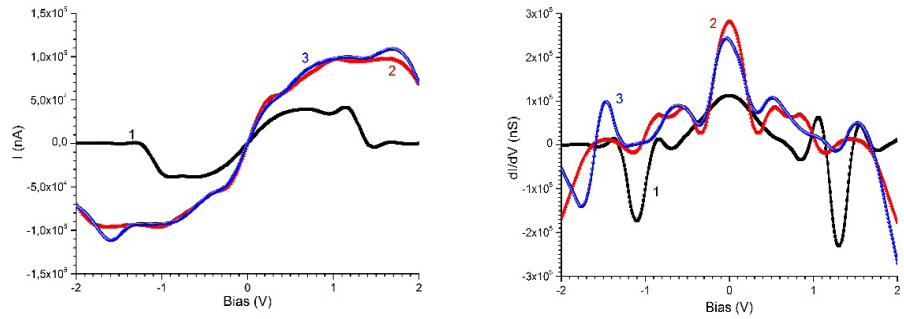

a) b)

Fig. 3. IV (a) and *dI/dV*-characteristics (b) of the FeSe monolayer (1 – non-stressed sample, 2 – stressed sample with a substrate, 3 – stressed sample without a substrate).

The graph clearly shows that in a stressed monolayer without a substrate, electronic transport is faster, since the stress period in it is less than in a stressed sample with a substrate.

Figure 4 shows the dependence of the second derivative (d^2I/dV_2) on the bias voltage. It characterises the features of electron-phonon interaction in the FeSe monolayer with different geometric structures, the influence of substrates on the properties of the sample, and the nature of quasiparticle tunnelling.

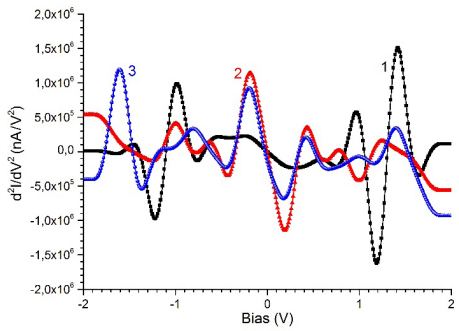

Fig. 4. d^2I/dV^2- characteristics (b) of the FeSe monolayer (1 – non-stressed sample, 2 – stressed sample with a substrate, 3 – stressed sample without a substrate).

Three distinct peaks were observed at -1 V, 1 V, and 1.5 V in a non-stressed sample (Fig. 4 (1)), relevant to the tunnelling conductivity of the FeSe sample. In the background structure of non-stressed sample, the background responsible for the electron-phonon interaction was observed at -0.8 V÷0.8 V. The dips at -1.2 and 1.2 V (Fig. 4 (1)) are associated with phonon processes and can be compared with the peaks of the fluctuation spectrum of the structure. The most distinct peaks relevant to tunnelling occurred in a stressed sample without a substrate. The depth of the minimum at 0.2 V in a stressed sample with a substrate was -12 $\mu A/V^2$ (Fig. 3(2)) and in a stressed sample without a substrate it was -0.6 $\mu A/V^2$ (Fig. 3(3)). Thus, the local minimum was enhanced in the sample when exposed to the substrate in the region of 0.2 V. In stressed samples, the electron-phonon mechanism of tunnelling conductivity prevailed and there were more peaks in the region of -1.8 V, -1÷0.7 V, 0.2 V, 0.5 V, 1.2 V÷1.4 V.

5. CONCLUSIONS

In this paper, the electric transport properties of the FeSe monolayer have been modelled in accordance with DFT + NEGF. Transmission spectra CVC, dI/dV, d^2I/dV^2 have been determined. It has been shown that the transmission of the nanostructure depends on the geometry of the sample and that the current flows well through the stressed film in contrast to the non-stressed one. The nature of sharp peaks in the transmission spectrum is related to resonant tunnelling of quasiparticles. On CVC of non-stressed sample, a section of NDR is observed in the range from -1.2 V to -1 and from 1.2 V to 1.4 V. NDR is shown at both signs of the applied voltage, which allows judging about the symmetry of the structure. Based on the second derivative of CVC, we can conclude that the phonon conduction mechanism is manifested in the non-stressed sample. There are three distinct maxima and two minima. It has been shown that the electron-phonon interaction is stronger in a stressed FeSe film than in the non-stressed, and that the frequency of local fluctuation increases when exposed to the $SrTiO_3$ substrate. The results obtained can be useful for the calculation of new promising electronic devices in 2D nanoelectronics.

ACKNOWLEDGEMENTS

The research has been supported by the grant of the Ministry of Education and Science of the Republic of Kazakhstan AP08052562. In addition, the research of AIP has been supported by the Latvian-Ukrainian Grant LV-UA/2018/2.

REFERENCES

1. Kyerematenga, N.A., Brousse, T., & Pech, D. (2017). Microsupercapacitors as Miniaturized Energy-Storage Components for On-Chip Electronics. *Nature Nanotechnology*, *12*, 7–15. DOI:10.1038/nnano.2016.196

2. Kreisel, A., Hirschfeld, P.J., & Andersen, B.M. (2020). On the Remarkable Superconductivity of FeSe and its Close Cousins. *Symmetry*, *12* (9), 1402. DOI:10.3390/sym12091402
3. Liu, C., & Zou, K. (2020). Tuning Stoichiometry and its Impact on Superconductivity of Monolayer and Multilayer FeSe on $SrTiO_3$. *Physical Review B*, *101* (14), 140502. DOI:10.1103/PhysRevB.101.140502
4. Chen, Y.H., Sun, Y., Ji, S.Y., Xiong, W., Pei, Z.C., & Wang, Z.W. (2020). Enhancement of Effective Masses of the Surface Polaron in FeSe Thin Film on $SrTiO_3$ Substrate. *Superlattices and Microstructures*, 106573. DOI:10.1016/j.spmi.2020.106573
5. Kozlovskiy, A., Zhanbotin, A., Zdorovets, M., Manakova, I., Ozernoy, A., Kadyrzhanov, K., & Rusakov, V. (2015). Study of Ni/Fe Nanotube Properties. *Nuclear Instruments and Methods in Physics Research Section B: Beam Interactions with Materials and Atoms*, *365*, 663–667. DOI:10.1016/j.nimb.2015.09.090
6. Zdorovets, M.V., & Kozlovskiy, A.L. (2018). Argon Ion Irradiation Effect on Zn Nanotubes. *Journal of Materials Science: Materials in Electronics*, *29* (5), 3621–3630. DOI:10.1007/s10854-017-8292-5
7. Zdorovets, M.V., & Kozlovskiy, A.L. (2019). Investigation of Phase Transformations and Corrosion Resistance in $Co/CoCo_2O_4$ Nanowires and their Potential Use as a Basis for Lithium-Ion Batteries. *Scientific Reports*, *9* (1), 1–12. DOI:10.1038/s41598-019-53368-y
8. Akilbekov, A., Akylbekova, A., Usseinov, A., Kozlovskyi, A., Baymukhanov, Z., Giniyatova, S., … & Dauletbekova, A. (2020). Ion Track Template Technique for Fabrication of $ZnSe_2O_5$ Nanocrystals. *Nuclear Instruments and Methods in Physics Research Section B: Beam Interactions with Materials and Atoms*, *476*, 10–13. DOI:10.1016/j.nimb.2020.04.039
9. Chen, C., Liu, C., Liu, Y., & Wang, J. (2020). Bosonic Mode and Impurity-Scattering in Monolayer Fe(Te,Se) High-Temperature Superconductors. *Nano Letters*, *20* (3), 2056–2061. DOI:10.1021/acs.nanolett.0c00028
10. Isherwood, L.H., Worsley, R.E., Casiraghi, C., & Baidak, A. (2018). Alpha Particle Irradiation of Bulk and Exfoliated MoS_2 and WS_2 Membranes. *Nuclear Instruments and Methods in Physics Research Section B: Beam Interactions with Materials and Atoms*, *435*, 180–189. DOI:10.1016/j.nimb.2018.01.018
11. Qiao, M., Wang, T.J., Zhang, J., Liu, Y., Liu, P., & Wang, X.L. (2018). The Effect of Carbon-Ion Irradiation on Surface Microstructure and Photoluminescence Properties in Monolayer Tungsten Diselenide. *Nuclear Instruments and Methods in Physics Research Section B: Beam Interactions with Materials and Atoms*, *435*, 278–284. DOI:10.1016/j.nimb.2018.01.003
12. Sergeyev, D.M. (2018). Computer Simulation of Electrical Characteristics of a Graphene Cluster with Stone-Wales Defects. *Journal of Nano and Electronic Physics, 10* (3), 03018. DOI:10.21272/jnep.10(3).03018
13. Dragoman, M.A., Dinescu, A., & Dragoman, D. (2019). 2D Materials Nanoelectronics: New Concepts, Fabrication, Characterization from Microwaves up to Optical Spectrum. *Phys. Status Solidi A,* 1800724. DOI:10.1002/pssa.201800724
14. Illarionov, Yu.Yu., Knobloch, T., Jech, M., Lanza, M., Akinwande, D., Vexler, M.I., … & Grasser, T. (2020). Insulators for 2D Nanoelectronics: the Gap to Bridge. *Nature Communications, 11*, 3385. DOI:10.1038/s41467-020-16640-8
15. Sergeyev, D., & Zhanturina, N. (2019). Simulation of Electrical Characteristics of Switching Nanostructures "Pt-TiO-Pt" and "Pt-NiO-Pt" with Memory. *Radioengineering, 28* (4), 714–720. DOI:10.13164/re.2019.0714
16. Liu, N., Bo, G., Liu,Y., Xu, X., Du, Y., & Dou, Sh. (2019). Recent Progress on Germanene and Functionalized Germanene: Preparation, Characterizations, Applications, and Challenges. *Small, 15* (32), 1805147. DOI:10.1002/smll.201805147

17. Huang, W.Q., Liu, Sh.R., Pen, H.Y., Li, X., & Huang, Z.M. (2020). Synthesis of New Silicene Structure and its Energy Band Properties. *Chinese Physics B,* 29, 084202. DOI:10.1088/1674-1056/ab942c
18. Kiraly, B., Liu, X., Wang, L., Zhang, Zh., Mannix, A.J., Fisher, B.L., … & Guisinger**,** N.P. **(2019).** Borophene Synthesis on Au(111). *ACS Nano*, *13* (4), 3816–3822. DOI:10.1021/acsnano.8b09339
19. Sahoo, S.K., & Wei, K.H. (2019). A Perspective on Recent Advances in 2D Stanene Nanosheets. *Advanced Materials Interfaces, 6* (18), 1900752. DOI:10.1002/admi.201900752
20. Pica, M., & D'Amato, R. (2020). Chemistry of Phosphorene: Synthesis, Functionalization and Biomedical Applications in an Update Review. *Inorganics, 8 (4), 29.* DOI:10.3390/inorganics8040029
21. Vergera, L., Xub, Ch., Natua, V., Cheng, H., Ren, W., & Barsouma, M.W. (2019). Overview of the Synthesis of MXenes and Other Ultrathin 2d Transition Metal Carbides and Nitrides. *Current Opinions in Solid State and Materials Science, 23* (3), 149–163. DOI*:*10.1016/j.cossms.2019.02.001
22. Meng, Zh., Stolz, R.M., Mendecki, L., & Mirica, K.A. (2019). Electrically-Transduced Chemical Sensors Based on Two-Dimensional Nanomaterials. *Chemical Reviews*, *119*, 478–598. DOI*:*10.1021/acs.chemrev.8b00311
23. Yu, J., Meng, L., Wu, J., & Li, Y. (2019). Correlation Effect on the Electronic Properties of Pair-Checkerboard AFM Monolayer FeSe: a First-Principles Study. *Journal of Phyics*: *Condensed Matter*, *31*, 305502. DOI:10.1088/1361-648X/ab1afb
24. Koch, R.J., Konstantinova, T., Abeykoon, M., Wang, A., Petrovic, C., Zhu, Y., … & Billinge, L. (2019). Room Temperature Local Nematicity in FeSe Superconductor. *Physical Review B 100*, 020501. DOI:10.1103/PhysRevB.100.020501
25. Jandke, J. Yang, F., Hlobil, P., Engelhardt, T., Rau, D., Zakeri, K., … & Wulfhekel, W. (2019). Unconventional Pairing in Single FeSe Layers*.* *Physical Review B 100*, 020503(R). DOI:10.1103/PhysRevB.100.020503
26. Coh, S., Cohen, M.L., & Louie, S.G. (2015). Large Electron–Phonon Interactions from FeSe Phonons in a Monolayer. *New Journal of Phys*ics, *17*, 073027. DOI:10.1088/1367-2630/17/7/073027.
27. Sergeyev, D. (2020) Single Electron Transistor Based on Endohedral Metallofullerenes Me@C_{60} (Me = Li, Na, K). *Journal of Nano and Electronic Physics, 12* (3), 03017. DOI:10.21272/jnep.12(3).03017
28. Sergeyev, D.M. (2020). Specific Features of Electron Transport in a Molecular Nanodevice Containing a Nitroamine Redox Center, *Technical Physics, 15* (4), 573–577. DOI:10.1134/S1063784220040180
29. Sergeyev, D.M., Myasnikova, L.N., & Shunkeyev, K.Sh. (2020). Computer Simulation of Spin Filtration Properties of Zigzag-Edged Octagraphene Nanoribbon Saturated with Hydrogen Atoms. *Russian Physics Journal*, *63*, 303–310. DOI:10.1007/s11182-020-02036-0
30. Atomistix ToolKit. Manual Version. (2015). *QuantumWise A/S, 1*, 840.
31. Ryczko, K., Strubbe, D.A., & Tamblyn, I. (2019). Deep Learning and Density-Functional Theory. *Physical Review A, 100, 022512.* DOI: 10.1103/PhysRevA.100.022512
32. Sergeyev, D. (2019). Computer Simulation of the Electrotransport Characteristics of the "Au – Bipyridine – Au" Nanocontact. *Journal of Nano and Electronic Physics, 11* (4), 04023 DOI:10.21272/jnep.11(4).04023
33. Gurvitz, S. (2019). Generalized Landauer Formula for Time-Dependent Potentials and Noise-Induced Zero-Bias DC Current. *Journal of Physics A: Mathematical and Theoretical, 52*, 175301. DOI:10.1088/1751-8121/ab10ed
34. Esmaeili, M., Jafari, M., & Sanaeepur, M. (2020). Negative Differential Resistance in Nanoscale Heterostructures Based on Zigzag Graphene Nanoribbons Anti-Symmetrically Decorated with BN. *Superlattices Microstructures*, *145,* 106584. DOI:10.1016/j.spmi.2020.106584

sciendo

LATVIAN JOURNAL OF PHYSICS
AND TECHNICAL SCIENCES
2020, N 6

DOI: 10.2478/lpts-2020-0030

RATED POWER DETERMINATION FOR AUTONOMOUS MICRO COMBINED HEAT AND POWER AND RECHARGEABLE BATTERY SYSTEM

A. Fedotov[1], G. Vagapov[1]*, L. Grackova[2]** and R. Abdullazyanov[1]

[1] Kazan State Power Engineering University, Department of Methods of Increase of Power Supply Reliability and Power Quality in Distributive Electrical Grids,
51 Krasnoselskaya St., Kazan, 420066, RUSSIA
*e-mail: vagapov@mail.ru
[2] Institute of Physical Energetics, Laboratory of Energy System Analysis and Optimisation,
11 Krīvu St., Riga, LV-1006, LATVIA
**e-mail: larisa.grackova@inbox.lv

An autonomous micro combined heat and power (Micro-CHP) is usually installed to increase energy efficiency and reduce energy costs in areas remote from large power systems. The main goal of autonomous Micro-CHP is to provide residential and industrial areas with electricity and heat. By designing an autonomous Micro-CHP, one of the key issues is the determination of rated power, since the energy efficiency of equipment and the costs of fossil fuels depend on the rated power. The mathematical model can better calculate the necessary rated power for an autonomous Micro-CHP in the case of operation with rechargeable batteries. Overall, the results have shown that the engine characteristics, operation process of three-phase synchronous generator and statistical information on loads are the criteria for improving energy efficiency.

Keywords: *Mathematical modelling, micro combined heat and power systems, rechargeable batteries.*

1. INTRODUCTION

Energy efficient consumption of energy resources is one of the goals of the national energy policy for all states. Effective use of energy, as well as expansion of consumer's awareness means increasing competitiveness in the industrial sector and reducing harmful emissions into the environment. One of the objects of efficient use of energy resources is autonomous micro-CHPs on fossil fuels (diesel, gas, etc.). Micro-CHPs generate simultaneously electricity and heat, thereby saving more than 40 % of fossil fuels compared to separate production of electrical and heat energy. Thus, decentralized production of electric and heat energy is economically advantageous in terms of reducing overall operating costs and carbon emissions [1]. Currently, the owners of autonomous Micro-CHPs are interested not only in production, but also in the accumulation of electrical energy in the period of time when consumption is reduced. It is the easiest way to save the generated electrical energy in high-capacity batteries (HCB). The use of rechargeable batteries for motor vehicles has significantly affected the expansion of their application in other production spheres. In particular, rechargeable batteries are already used in important power supply systems for temporary uninterrupted operation, allowing the backup diesel generators to enter a given operating mode. In addition, micro-CHP stations, such as gas piston installations (GPI), together with rechargeable batteries are fuel-saving idle-stop and switch from one mode to another, thereby reducing the wear of turbines and the efficiency of the turbine increases. It also ensures uninterrupted and efficient operation of GPI with a sharp decrease or increase in load.

The aim of this paper is to estimate the necessary rated power of autonomous Micro-CHP in the case of joint operation with high-capacity storage battery.

2. PROFILES OF ELECTRICITY CONSUMPTION

An autonomous Micro-CHP is customary to choose according to the rules of design and erection of electrical equipment of residential and public buildings, the standard curves of the load variation during the day and the forecast of energy consumption for the next several years. For the study, the analysis of seasonal and daily energy consumption in household, social and service sectors (statistical data from 2010 to 2019 of the Republic of Tatarstan (Russian) [2] and Latvian [3]) has been performed, which showed that the maximum power consumption occurs during the winter season.

Figures 1–3 show examples of actual load variation curves during a day for separate consumer categories in a working day, which have been chosen as they directly represent a large number of customers in the autonomous territories. The objects have been classified into three respective sectors: the household sector, the social sector and the services sector. The database of the quantitative indicators and load graphs of the six objects of each type have been investigated. Figure 1 demonstrates the household sector, i.e., consumers of private and dwelling houses. The social sector is represented by school and kindergarten consumers (see Fig. 2), while the services

sector is made up by consumers of catering establishments and stores (see Fig. 3).

Maximum and minimum daily electricity consumption for each object, as well as the load factor has been determined.

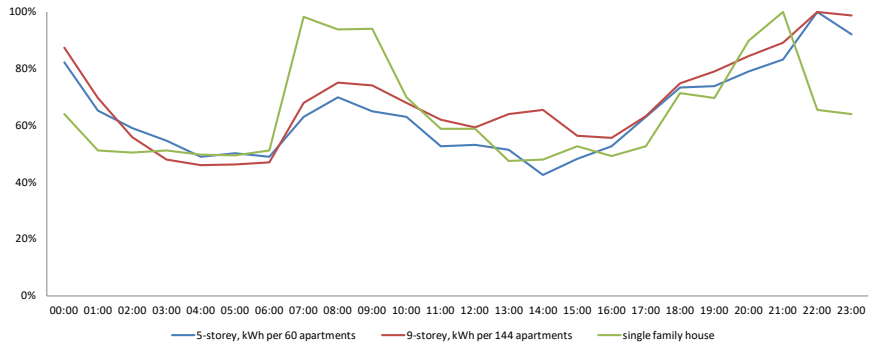

Fig. 1. Daily variation curves of the household sector.

Figure 1 shows the household sector, where we can observe that for the private house the maximum consumption is from 07:00 to 10:00 and from 18:00 to 22:00, the minimum consumption is from 10:00 to 18:00 and from 22:00 to 07:00. The demand factor is 0.65. For a 5-storey dwelling house, the maximum consumption is from 07:00 to 10:00 and from 17:00 to 01:00, the minimum consumption is from 10:00 to 17:00 and from 01:00 to 07:00. The demand factor is 0.64. For a 9-storey dwelling house, the maximum consumption is from 07:00 to 10:00 and from 18:00 to 02:00, the minimum consumption is from 10:00 to 18:00 and from 01:00 to 07:00. The demand factor of the household sector (f_{dhs}) is 0.68.

The average maximum total loads are presented by the following values:

- 5-storey building (60 apartments) $P_{max\ actual}$ = 54 kW;
- 9-storey building (144 apartments): $P_{max\ actual}$ = 93 kW;
- private house (with gas heating): $P_{max\ actual}$ = 7.5 kW.

For the household sector, the peak demand occurs from 07:00 to 10:00 and from 18:00 to 23:00. The calculated average demand factor of the household sector is 0.656.

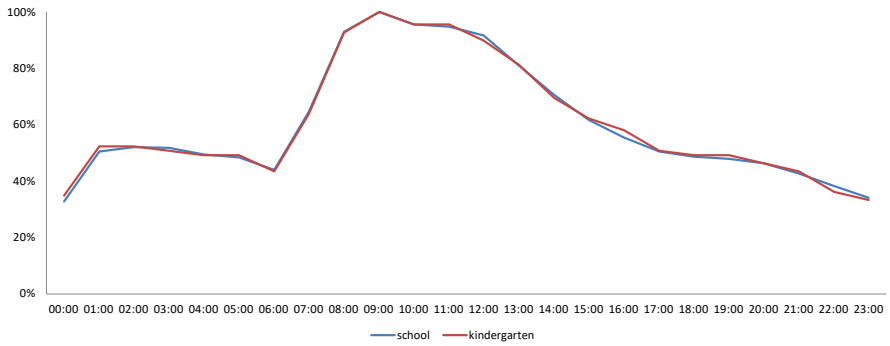

Fig. 2. Daily variation curves of the social sector.

Comparing the results of the electricity consumption profiles shown in Fig. 2, one can see the maximum load during the period from 07:00 to 15:00 in the social sector. The demand factor of the social sector (f_{dsocs}) is 0.60.

The average maximum total loads are presented by the following values:

- a school with 1852 students: $P_{max\ actual}$ = 718 kW;
- a kindergarten for 54 children: $P_{max\ actual}$ = 176 kW.

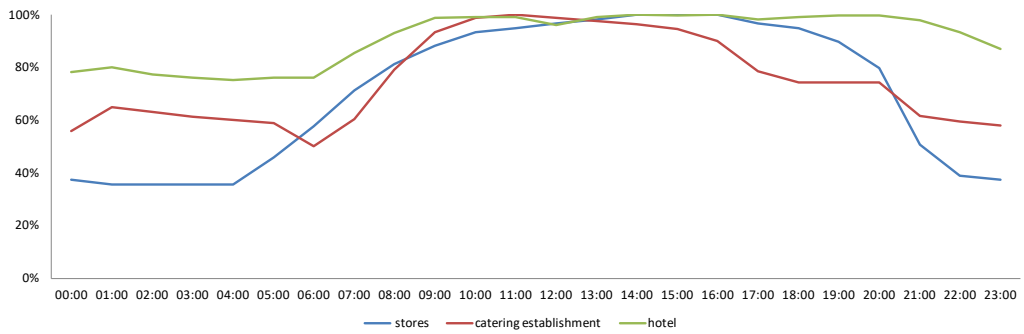

Fig. 3. Daily variation curves of the services sector.

In the services sector for the hotels the peak and on-peak demand are not expressed, the demand factor is in the range of 0.91, indicating that the load is evenly distributed throughout the day. For the catering establishments and the stores, the maximum consumption is from 07:30 to 20:30. The demand factor is 0.71 and 0.75, respectively. The calculated average demand factor of the commercial sector (f_{dcs}) is 0.79.

The average maximum total loads are presented by the following values:

- hotel – 187 m^2: $P_{max\ actual}$ = 27 kW;
- store – 1500 m^2: $P_{max\ actual}$ = 334 kW;
- catering establishments – 565 m^2: $P_{max\ actual}$ = 258 kW.

All in all, it can be concluded that for the considered consumer categories the largest maximum demand of electricity is observed from 07:00 to 22:00, whereas from 23:00 to 07:00 there is the minimum demand. Granted, not all of these objects will be on at the same time but the wattage capacity needs to be there for the peak load.

The total load and the schedule on the autonomous micro combined heat and power from the consumer groups are determined by (1):

$$\sum_{i=1}^{i=n} P_i = P_{hs} f_{dhs} + P_{socs} f_{dsocs} + P_{ss} f_{dss}\ , \quad (1)$$

where

P_{hs} is load from the household sector and f_{dhs} is the average load factor from the household sector;

P_{socs} is load from the social sector and f_{dsocs} is the average load factor from the social sector;

P_{ss} is load from the services sector and f_{dss} is the average load factor from the services sector.

The load factor (f_{load}) shows the extent of use of the active power for the load curve in a specified time period and is determined by (2):

$$f_{load} = \frac{t_1 P_1 + t_2 P_2 + ... + t_{24} P_{24}}{\left(t_1 + t_2 + ... + t_{24}\right) P_{\max}} = \frac{1}{t P_{\max}} \int_0^{24} P(t) . \quad (2)$$

According to the above-mentioned figures and expressions and also by the method of converting daily load schedules into equivalent daily two-stage schedules, the rated power of an autonomous Micro-CHP can be determined.

3. THE COMBINED USE OF AN AUTONOMOUS MICRO-CHP WITH HIGH-CAPACITY STORAGE BATTERY

The rated power of an autonomous Micro-CHP without or with rechargeable batteries is recommended to be selected according to the expected maximum load, taking into account the technical characteristics of the engine [4].

The rated power is determined according to the profiles of electricity consumption, which have been discussed above as examples of the load of objects. When designing an autonomous Micro-CHP with high-capacity storage battery, the charge and discharge process of rechargeable batteries is considered according to the criterion of the minimum daily fuel consumption Q_s, which depends on the load schedule and fuel consumption characteristics for the engine, provided that during the day the rechargeable battery charge is consumed in full [5]. Based on the information above, we simulate the joint operation of an autonomous micro-CHP and a battery, the charging of which occurs during the period of minimum daily load of a residential area.

A. Mathematical Modelling

Figure 4 shows a two-stage load graph, where P_{L1} is the minimum load in the time interval [0; $T - T_m$], P_{L2} – the maximum load of duration Tm, respectively, in the time interval [$T - T_m$; T]. One of the important conditions for minimising fuel consumption for power plants during parallel operation is the distribution of the total load between them. Using the method of Lagrange multipliers for the time interval [0; T], we obtain restrictions for determining the power of high-capacity storage battery. The total fuel consumption Qs ([0; T]), which consists of the fuel consumption Q_1 in the interval [0; $T - T_m$] at P_1 of the power of the power plant for the load P_{L1}, and Q_2 at the interval [$T - T_m$; T] at P_2 power of the power plant to the load P_{L2}, can be written as (3):

$$Q_S = Q_1 + Q_2 . \quad (3)$$

Then the Lagrange function takes the following form (4):

$$Q_S = Q_1 + Q_2 + \lambda_1 W_1 + \lambda_2 W_2 + \lambda_3 W_3 \to \min , \quad (4)$$

where according to the energy balance, energy restrictions W_i are written as (5):

$$\left.\begin{aligned} W_1 &= \eta\left(P_1 - P_{L1}\right)\left(T - T_m\right) - P_{x1}\left(T - T_m\right) = 0, \\ W_2 &= \left(P_2 - P_{L2}\right)T_m - \eta P_{x2} T_m = 0, \\ W_3 &= P_{x1}\left(T - T_m\right) - P_{x2} T_m = 0. \end{aligned}\right\}, \tag{5}$$

where P_{x1} and P_{x2} are charge power of the high-capacity storage battery (HCSB) and the HCSB discharge power, respectively, η is the efficiency of the charge – HCSB charge process.

The joint work of the power plant and HCSB is illustrated in Fig. 4.

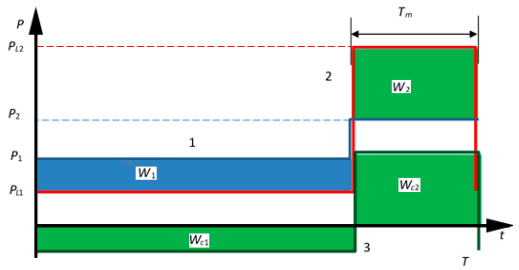

Fig. 4. Equivalent daily two-stage load schedule.

1 – power plant capacity; 2 – daily load schedule; 3 – load schedule of high-capacity storage battery; W_1 – electric power transmission from the power plant for HCSB; W_2 – electric power transmission from the HCSB for power plant; W_{c1} – power accumulated from power plant to HCSB; W_{c2} – HCSB power supplied to the power plant.

The charge process of high-capacity storage battery occurs at the minimum daily load and, taking into account losses, energy storage is defined as $W_{c1} = \eta W_1$. When the load increases to P_{L2}, discharge occurs of the HCSB, which is additional power for autonomous Micro-CHP. The discharge process, taking into account losses, is defined as $W_2 = \eta W c_2$. The capacity of high-capacity storage battery is defined as $P_h = P_{L2} - P_2$, where P_2 is the rated power of the power plant and P_h is the power of the HCSB.

The operating mode of the batteries has been modelled using the Simulink Simscape Power Systems (Battery block) [6]. The parameters of the Li-ion high-capacity storage battery are derived from the discharge characteristics. The discharging and charging characteristics are assumed to be the same. The maximum allowable battery depth of discharge is 20 %.

Applying Eqs. (4) and (5), we find the extremes Qs according to Eq. (6):

Capacity of the battery storage

$$-\lambda_3 = \frac{1}{\eta}\frac{\partial Q_1}{\partial P_1}\frac{1}{T - T_m} = \eta\frac{\partial Q_2}{\partial P_2}\frac{1}{T_m}. \tag{6}$$

Fuel consumption q for each hour is determined by Eq. (7):

$$\frac{\partial Q_1}{\partial P_1}\frac{1}{T - T_m} = \frac{\partial q_1}{\partial P_1} = \eta^2\frac{\partial q_2}{\partial P_1} = \eta^2\frac{\partial Q_2}{\partial P_2}\frac{1}{T_m}. \tag{7}$$

Taking into account the restrictions for the energy balance (Eq. 5), the total capacity of the power plant in time intervals is determined by:

$$P_2 = P_{L2} + \frac{\left(P_{L1} - P_1\right)}{\rho}, \quad \rho = \frac{T_m}{\eta^2\left(T - T_m\right)} \quad \text{and} \quad P_{x2} = \frac{P_{L2} - P_2}{\eta}, \tag{8}$$

where ρ is a relative value of the duration of the maximum load and P_{x2} is maximum power of HCSB in the discharge mode.

The total installed capacity of an autonomous Micro-CHP with rechargeable batteries and the optimum load are calculated using Eq. (7). The fuel rate in the analytical formula is defined as $q = a + bP^{\mu}$ (litre/hour). Based on the fuel consumption characteristics of a particular power plant (Block 1), a three-phase synchronous generator (Block 3) and actual load (Block 5) approximation coefficients a, b and μ are selected. For this purpose, using Simulink Simscape Power Systems, the distribution network has been modelled and tested in the discrete mode (see Fig. 5).

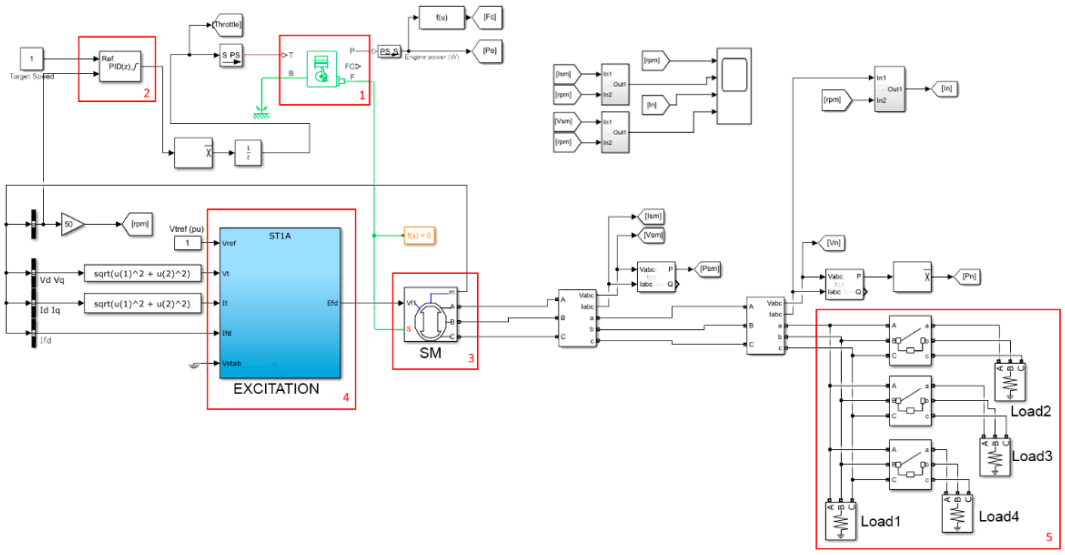

Fig. 5. Distribution network model "Engine – three-phase synchronous generator – Load".

Block 1: Engine characteristics definition.
Block 2: Differential controller of engine speed.
Block 3: Three-phase synchronous generator.
Block 4: Generator excitation system.
Block 5: Actual load: 100 %, 75 %, 50 % and 25 %.

Then, minimum power plant P_1 is determined as the correlation between the generated power at the minimum fuel consumption and time intervals:

$$P_1 = \eta^{2/\mu - 1} P_2 . \tag{9}$$

Applying Eq. (8), the maximum power plant (P_2) is determined by:

$$P_2 = \frac{P_{L1} + \rho P_{L2}}{\eta^{2/\mu - 1} + \rho} = P_{L2} \frac{k_m^{-1} + \rho}{\eta^{2/\mu - 1} + \rho}, \quad \text{where} \quad k_m = \frac{P_{L2}}{P_{L1}} . \tag{10}$$

Total fuel consumption Qs in the time interval [0; T] is calculated as follows:

$$Q_s = aT + b\left[P_1^{\mu^*}\left(T - T_m\right) + P_2^{\mu^*} T_m\right]. \quad (11)$$

Thus, we can conclude that Eq. (7)–(11) allow determining the rated power of the power plant with minimum fuel consumption (Q_s).

B. Math Model Testing

Thus, to validate the mathematical model, two work modes have been simulated:

- Work mode A is a model of the autonomous Micro-CHP (diesel generator DOOSAN DP158LD, 0.424 MW rated power);
- Work mode B is a model of the autonomous Micro-CHP diesel generator DOOSAN DP158LD, 0.424 MW rated power) with rechargeable batteries.

The input data of mode A are as follows: P_2 = 0.422 MW; km = 5; T = 24 hours; T_{max} = 4 hours. μ = 1.45 (p.u); a = 22.31 (liter/hour); b = 368.57 (liter/kWh) and 25 % actual load.

On the basis of this information, the minimum daily load for the temporary daily intervals is calculated by Eq. (10). Therefore, P_{L1} = 0.4/5 = 0.08 MW and P_{L2} = 0.4 MW.

The total fuel consumption Qs in the time interval [T – Tm; T] has been defined by Eq. (11):

$$Q_s = 22.31 \cdot 24 + 368.57\left[0.08^{\,1.45} \cdot \left(24 - 4\right) + 0.4^{\,1.45} \cdot \left(24 - 4\right)\right] = 1115 \text{ liter}.$$

Further, taking into account input data of mode A and the main characteristics of Lithium-Ion (Li-Ion) rechargeable batteries (where η^2 = 0.9, ρ =0.222 and $\eta^{2/\mu-1}$ = 0.791), mode B has been calculated.

Applying Eq. (8), the maximum power plant (P_2) is determined as follows:

$$P_2 = 0.4\frac{5^{-1} + 0.222}{0.791 + 0.222} = 0.167MW.$$

The minimum power plant (P_1) is estimated by Eq. (9):

$$P_1 = 0.791 \cdot 0.167 = 0.132MW.$$

The results show that it is necessary to use a diesel generator of lower power. Since, according to the requirements of the operating conditions, the power plant of the diesel generator must have a power reserve of at least 30 % of the required consumption, diesel generator G299BDGR (0.217 MW rated power) has been selected from the list of industrial diesel generators.

However, when the load increases to P_{L2} = 0.4 MW, the process of discharge of the HCSB is carried out. In our case, the capacity of high-capacity storage battery is defined by Eq. (10):

$$P_{x2} = \frac{0.4 - 0.167}{0.95} = 0.246MW .$$

According to the requirements of the manufacturers, for maximum life, the battery should not be discharged by more than 40 %. Therefore, LT-LYP 380 lithium iron phosphate batteries have been selected. In our case, the discharge process takes place within four hours and the charging process will be carried out within 20 hours a day.

Total fuel consumption *Qs* in the time interval [0; T] is calculated as follows:

$$Q_s = 22.31 \cdot 24 + 368.57\left[0.132^{\,1.45} \cdot (24 - 4) + 0.167^{\,1.45} \cdot (4)\right] = 1035 \text{ liter} .$$

The calculations above allow concluding that when using rechargeable batteries at peak loads, it will be enough to install diesel generators with a capacity of 0.217 MW, which will reduce diesel consumption by 68 tonnes per day or 24820 tonnes per year. In addition, using a high-capacity storage battery results in a reduction of diesel fuel costs of about €14.15 million per year. In turn, this also leads to emission reduction, i.e., a decrease in 78.15 thousand tons of CO_2 emissions each year (see Table 1).

Table 1. Output Data of Mode A and Mode B

	Work mode A	Work mode B
Qs, kt/year	345.93	321.11
Qs, TJ/year	14698.51	13643.91
Qs, EUR million per year. Diesel fuel price per 1 tonne = 570 EUR. April 2020. [7]	197.18	183.03
CO2, kt/year [8]	1089.160	1011.014

Comparing the results of the modelled modes of the data on the fuel consumption, one can see that mode 2 is favourable as to the fuel consumption and CO_2 emissions from fossil fuel. Fuel consumption and CO_2 emissions decreased by 7.2 % using a diesel generator of lower power.

The results of the modelled modes allow concluding that despite a similar load it is possible to cut fuel consumption and the volume of relevant emissions.

It should be noted that in the framework of the implementation of the project "Methods to Improve the Reliability of Power Supply Systems and the Quality of Electricity Based on Electrochemical Storage Devices and Digital Monitoring of the State of Distribution Electric Networks", an autonomous Micro-CHP with rechargeable batteries has been commissioned (Tomsk Region, federal subject of Russia, 2019). The main parameters of Micro-CHP are as follows: Caterpillar 3512 Diesel Generator, 0.980 MW rated power, average fuel consumption is 280 litre/hour; LiFePO4 batteries, 0.3 MVA installed capacity. Some images of the object are shown in Fig. 6.

An autonomous Micro-CHP

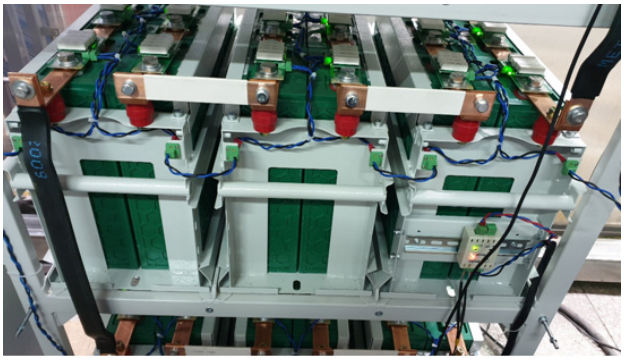

Battery configurations in sections

The control switchboard

Fig. 6. The images of autonomous Micro-CHP.

4. CONCLUSION

Choosing the capacity and planning the operation of an autonomous Micro-CHP must be based on technical and statistical information on loads. This means that equipment and energy resources will be used efficiently.

Taken together the theoretical and practical studies, it has been found that the efficient operation process of the autonomous Micro-CHP diesel generator and high-capacity storage battery can save fossil fuel and thereby reduce CO_2 emissions.

To make decisions on investment in an autonomous Micro-CHP diesel generator with high-capacity storage battery projects, it is necessary to consider a number of additional parameters that have not been examined in the article, for example, capital investments in a specific project to make forecast of fossil fuel cost for the next ten years. The variation in fossil fuel cost is influenced by a number of factors, such as social and economic changes in the country, world prices for fossil fuels, the tax system, etc.

The mathematical modelling considered in the article makes it possible to recognise this option of energy supply as effective in those areas where building the high voltage transmission and distribution lines is not economically profitable.

It should also be noted that for areas located close to the places of crude oil production, it is advisable to use associated gas as fuel, since here this type of fuel will have minimum cost. In terms of the investment and fossil fuel saving, substantial benefits could accrue.

ACKNOWLEDGEMENTS

The research has been supported by the Ministry of Science and Higher Education of the Russian Federation on fundamental scientific research "Distributed automated systems for monitoring and diagnostic the technical condition of overhead power lines and substations based on technology of broadband data transmission through power lines and the Industrial Internet of Things" (theme mnemonic code 0672-2020-0009, Agreement 075-03-2020-178).

REFERENCES

1. Mutule, A., & Teremranova, J. (2018). Introduction of Energy Saving Principles: Technologies and Awareness, Latvian Experience. *Latvian Journal of Physics and Technical Sciences, 55* (6), 52–62. DOI: 10.2478/lpts-2018-0044
2. Network Company. The Distribution System Operator in the Republic of Tatarstan. (n.d.) Retrieved 4 April 2020 from http://www.gridcom-rt.ru/o-kompanii/obshchaya-informatsiya
3. Latvenergo Group. (n.d.) Retrieved 5 December 2018 from http://www.latvenergo.lv/portal/page/portal/Latvian/Sad_tikls/Tipveida+grafiki_jauns.htm
4. Genmotors. (n.d.) Available at https://kazan.dizelnye-generatory.com/dizelnye-generatory/g584dsgr-grupel/
5. Promelektroautomatika. (n.d.) Available at http://www.pea.ru/docs/equipment/batteries/lioteh/
6. MathWorks. Simulink Simscape Power Systems (SimPowerSystems). Available at https://uk.mathworks.com/products/simpower.html
7. GlobalPetrolPrices.com. (n.d.) Available at https://www.globalpetrolprices.com/Russia/diesel_prices/
8. 2006 IPCC Guidelines for National Greenhouse Gas Inventories. Chapter 2: Stationary Combustion. (n.d.). Available at www.ipcc-nggip.iges.or.jp/public/2006gl/pdf/2_Volume2/V2_2_Ch2_Stationary_Combustion.pdf

sciendo

LATVIAN JOURNAL OF PHYSICS
AND TECHNICAL SCIENCES
2020, N 6

DOI: 10.2478/lpts-2020-0031

THE DEVELOPMENT OF THE SMART GAS DISTRIBUTION: GENERAL TRENDS AND THE LATVIAN CONTEXT

J. Savickis[1], L. Zemite[2*], L. Jansons[2] I. Bode[2], E. Dzelzitis[2],
A. Broks[2], L. Vempere[2]

[1]ITERA Latvija
50 Skanstes Str., Riga, LV-1013, LATVIA
[2]Riga Technical University,
Faculty of Electrical and Environmental Engineering,
Institute of Power Engineering
12-1 Azenes Str., Riga, LV-1048, LATVIA
*e-mail: laila.zemite@rtu.lv

A necessity to reduce greenhouse gas (hereinafter – GHG) emissions and energy import dependency, while coping with increasing energy demand, affordability issues and many other factors, causes the European Union (hereinafter – EU) energy policy makers to identify development trends that would help harmonize future energy market and technological changes with ever growing pressure of universal data processing digitalisation. In order to stimulate data processing digitalisation in energy, the European Commission has proclaimed a support to the development of all kind of the smart energy systems, where simultaneous use of the natural gas and renewable gases (hereinafter – RG) will play one of the major sustainability ensuring roles. Firstly, it will help achieve designated energy efficiency goals and, secondly, enable cost saving synergetic solutions at the early stages of the energy supply chain decarbonisation.

Synergy of the natural gas and RG emphasises the need for a modern, smart and sustainable energy infrastructure to allow developing more flexible back-up and balancing power capacity, storage solutions and innovative demand-response mechanisms.

This paper addresses some trends in development of the smart gas distribution (hereinafter – SGD) as part of the smart energy systems both in the EU and Latvia, with a particular focus on smart energy concepts, smart gas metering and grid modernisation.

Keywords: *Natural gas, smart energy systems, smart gas distribution, smart gas metering, synergy.*

1. INTRODUCTION

The natural gas is the second largest source of energy in the EU, which has provided between 23 % and 26 % of the European energy mix over the past two decades [1]. Its consumption is a subject to change on a yearly basis, and the greatest drivers of these changes are typically economic factors and weather conditions rather than structural energy supply chain transformations. Therefore, the present stability of the natural gas in the EU energy sector is determined by several key factors, such as cost competitiveness, security of supply, overall accessibility and sustainability [2].

The statistics shows that consumption of the natural gas in the EU has been quite stable also in recent few years, even demonstrating signs of some positive dynamics. In 2017, gross consumption of the natural gas in the EU increased by 3.7 % in comparison with 2016, to reach 18 587 thousand terajoules, but its use in the European energy production continued to demonstrate a downward pattern [3], [4].

For large-scale natural gas infrastructure in the EU, in order to stay relevant, fulfillment of additional functions beyond its traditional role of transporting fossil fuel is expected. Sustainability of the future natural gas networks will increasingly depend on their versatility, flexibility, and pricing of such commodities as carbon dioxide (hereinafter – CO_2) emissions and land use. Europe's natural gas infrastructure is a valuable asset, which should not be only preserved for sake of preservation, but used rationally to increase energy sector overall sustainability and enhance security of energy supply. The possibility to establish dynamic, integrated synergy between natural gas – regardless of its transportation means and final consumption sector – and RES in form of the RGs till 2030 and beyond will define its role in the EU's decarbonised energy future for decades to come [5], [6].

The average natural gas price at key trading hubs of Europe normally ranges between 5 and 8 US dollars per million British thermal units or 17 and 27.2 US dollars per megawatt hour, which refers both to pipeline supply routes and liquefied natural gas (hereinafter – LNG) import [7]. In power generation, the natural gas has been cheaper than coal across the EU energy markets since late 2018, when the prices of CO_2 emission allowances began to increase after several years of freefall [8]. The natural gas is cost effective and can present a viable alternative not only to coal, but also to growing role of electricity in industrial, commercial and residential power supply. In 2018, the average natural gas price for household consumers in the EU was 0.06 euro per kilowatt hour (hereinafter – EUR/kWh), while electricity price in the same sector averaged 0.21 EUR/kWh. Similarly, the natural gas price for commercial customers averaged 0.04 EUR/kWh and electricity price for commercial customers – 0.14 EUR/kWh [9]. In all, on a levelised cost of service basis, the price of the natural gas in Europe for different groups of consumers was 30 to 50 % less than the price of electricity [10].

In regard to security of supply, it must be pointed out that half of all the natural gas supplies in Europe come from outside the EU region. Given the declining local natural gas production, the share of supplies from the Russian Federation to the EU Member States alone has grown from 35.2 % in 2010 to 40 % in 2018 [11]. However, supply of the natural gas in Europe is

relatively flexible, as multiple pipeline and LNG supply routes are available from the other third countries, including Algeria, the US, Qatar, Azerbaijan, and Libya. Notably, the share of LNG in the EU's natural gas supply structure is increasing rapidly: six new European countries have started importing LNG since 2010, but utilisation of regasification capacity has remained low, averaging less than 30 % over the past five years [1].

As for sustainability, the natural gas has already contributed to lower GHG emissions in Europe, but air pollution still remains one of the key environmental challenges, especially within cities. The latest European Environment Agency estimates show that fine particulate air pollution alone was responsible for about 400 000 premature deaths in European countries in 2016. Nitrogen dioxide emissions are also estimated to have caused 79 000 premature deaths in the same countries [12]. Fuel switching to the natural gas from coal in the power sector and diesel in the transport sector is widely acknowledged as one of the potential solutions to these problems. Since 2010, coal-to-gas switching has saved around 500 million tonnes of CO_2 as well – an effect equivalent to putting an extra 200 million EVs running on zero-carbon electricity on the road over the same period [13].

In mid- and long-term perspective, in order to ensure further utilisation of the existing natural gas infrastructure and decarbonisation of the EU energy sector, smart solutions and simultaneous use of RGs and the natural gas, with gradually decreasing percentage of the latter, are expected to be the key development drivers. Given that the necessity for smart transformation will be valid not only to the natural gas transportation and storage but also to the distribution level, the natural gas distribution industry will have to prepare itself to face the major novelties in the next two or three decades. Enabling technologies for data collection, analytics, and automation must motivate utilities to step back and take a comprehensive, critical view of their present infrastructure and operational activities, and thus welcome unavoidable modernisation of the natural gas distribution with regard to gradual transition to SGD [14].

It is quite challenging to predict with absolute certainty what the future may hold, once SGD becomes a reality because at the moment none of the EU Member States has a natural gas distribution system, which could be called truly smart. In fact, concepts of "smart energy systems" and "smart gas distribution" are still being defined [15]. Currently, only some elements of the SGD are present at the natural gas distribution level in Europe, such as more or less advanced smart metering and partial incorporation of RG production units into the natural gas grids. Moreover, incorporation of RG production units into the natural gas grids almost exclusively relates to biomethane production and injection into the natural gas grids at the distribution level. The RG supply diversification inputs of hydrogen are rare and sporadic [16].

The natural gas industries in many EU Member States are keen to gain more clarity and begin making necessary preparations for capturing the benefits from implementation of the SGD. It is important to be aware of the way the future of the natural gas distribution sector could look like when all major components of the SGD are puzzled together, and of the way the utilities get started with building out local SGD systems themselves. In addition, they should be developed with maximum preservation of the existing natural gas distribution infrastructure and benefits to consumers. These aspects are important not only at the

energy policy and strategy planning level in the leading EU Member States, but also in small countries, such as Latvia.

2. CONCEPTS OF THE SMART ENERGY SYSTEMS AND THE SGD

2.1. Definition and Content of Concepts

The concept "smart energy systems" is widely used by energy professionals in numerous contexts as it was introduced in order to identify potential synergy points among different segments of the energy sector. Some researches specify that smart energy systems are cost-effective, sustainable and secure energy systems in which renewable energy (hereinafter – RE) production, infrastructures and consumption are integrated and coordinated through energy services, active consumers (prosumers) and enabling technologies [15], [17]. Smart energy systems can be all inclusive or entirely based on the use of RE. The principal differences of conventional and smart energy systems are shown in Table 1.

Table 1. Principal Elements of Conventional and Smart Energy Systems

Conventional energy system	Smart energy system
Electromechanical meters	Digital meters
One-way communication	Two-way communication
Few sensors	Multiple sensors
Fully manual maintenance	Mostly automatic maintenance
Manual monitoring	Automatic monitoring
Limited control	Unlimited control
Impossible dynamic system and energy consumption data access	Possible dynamic system and energy consumption data access, including near real-time and real-time remote meter performance analysis
Manually generated bills	Automatically generated bills
Impossible use in the SGD and integrated energy systems	Unlimited use in the SGD and integrated energy systems

Unlike "smart grid" and "smart networks", which mostly deal with grid automation only, the smart energy systems cover the entire spectrum of energy production, transportation, distribution, storage and consumption. [15] In case of natural gas, smart energy systems may also hold significant exploitation potential of the Internet of Things (hereinafter – IoT), which can initiate new correlation models by supporting not only methodological and engineering, but also economic synergy across different segments of the energy sector [18].

One of the pathways currently demonstrating dynamic synergy of two energy sector segments, namely, electricity and gas, is power-to-gas (hereinafter – P2G) technology, which mostly defines RE storage in a form of such gaseous fuels as biomethane and hydrogen. In all, P2G is a technology that uses electricity to produce a gaseous fuel and allows electricity to be stored and transported in the form of compressed gas, often using existing natural gas transport,

storage and distribution infrastructure. P2G is often considered to be one of the most promising technology for seasonal RE storage [19].

A concept of the SGD therefore should be perceived as an integral part of emerging smart energy systems, and major estimated benefits of the SGD are as follows:

- lowering GHG emissions;
- decreasing the natural gas import dependency and improvement of the energy security of supply [20];
- increasing a share of RE (biomethane, hydrogen, syngas etc.) in the overall energy mix;
- improving energy efficiency by enabling active participation of the energy consumers (prosumer strategy) [21];
- creating conditions for efficient use of energy grids, thus giving consumers the ability to choose the most economic energy source in near real-time regime;
- avoiding additional investments in electricity networks by effective usage of existing gas grids, technologies and appliances;
- enabling synergies between gas and electricity sectors through encouragement of distributed generation [22].

There is not a widely accepted definition of the SGD either in the EU member states or in other countries of the world. For the purpose of clarity, in this paper a concept of the SGD is presented as a blend of three conjoined elements:

- the implementation of a range of new technologies to provide near real-time information about the end-to-end distribution system;
- analytics that allows for rapid decision making aligned with both a proactive approach to pipeline safety and overall operational efficiency;
- automated controls to help optimise both pipeline safety and efficiency [14].

The principal elements of the SGD are listed in Fig. 1. This scheme does not include multi-dimensional communication links among single elements of the system.

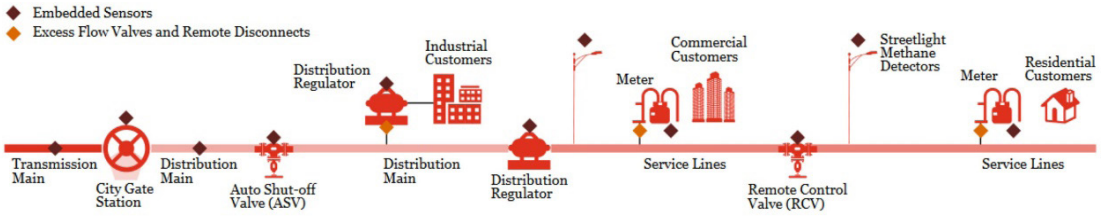

Fig. 1. Principal scheme of the SGD.
Source: *PwC*

2.2. Potential Disruptors of the SGD

New technologies are expected to change gas distribution operations fundamentally: smart sensors, controllers, and inspection technologies are being integrated with pipelines, valves, regulators, gas metering points/stations and gas meters to provide comprehensive, near real-time system information and unprecedented control of system operations. In addition, data from single smart system components, consolidated and analysed in the cloud, feed the SCADA system to allow for real-time opti-

misation of system operations as well [23]. It means that the SGD should not be evaluated in isolation, as system and data integration may be the most challenging aspect in its creation and enhancement. On the other hand, at the level of hardware, individual sensors or controllers cannot have a system-level impact without being integrated.

However, integration of data with operation, maintenance, and inspection information in the systems could trigger certain risks and challenges of integrity management, as well as better work planning and execution. Risks or potential disruptors of the SGD listed below fall into four main categories: smart pipeline and mobile technologies, advanced controls and automation, systems and records, and data processing and analysis.

Table 2. Potential Disruptors of the SGD

Category	Potential source of disruption
Smart pipeline and mobile technology	• Embedded sensors, inline robots – pipeline inspection gauges and ultrasonic inspection devices connected to SCADA • Remote leak detection by means of a car or other mobile technology, such as drones • Smart gas meters with expanded functionality and connectivity to other transmission networks • Mobile devices with secure connection to cloud-based information exchange and storage systems
Advanced controls and automation	• Remote control valves and automated shut-off valves connected to SCADA • Excess flow valves and remote disconnects integrated into smart gas meters • Natural gas distribution system visualization in the natural gas operations control centre
Systems and records	• Materials traceability • Enterprise system integration, including geographic information system, enterprise asset management, etc. • Data, records, and information management, including automated validation to ensure ongoing information quality
Data processing and analytics	• Analytics for all sources of information and relevant external sources of environmental information (e.g., weather, soil, seismography, traffic, etc.) • Tools for dynamic risk modelling and work prioritisation based on threat probability and consequence • Data archiving, safe keeping and on-demand traceability hubs

3. KEY EVALUATION FACTORS OF THE SGD AND SMART METERING

3.1. Key Evaluation Factors of the SGD

Emerging SGD calls for comprehensive planning that considers development of the natural gas distribution along three dimensions, which, at the same time, pose themselves as its key evolution factors: pipeline safety, risk-based integrity and asset management, and efficient, smart-tech-enabled consumer operations.

The impact of these three factors are described in Table 3 with regard to comparison of the current situation and theoretical estimates after implementation of the SDG.

Table 3. Key Evolution Factors for the SGD

Key factor	Current situation	Estimates after implementation of SGD
Pipeline safety	• Compliance-driven risk and activity management • Pipeline replacement, pressure testing, and capital projects carried out as special programmes • Mid-term investment programmes based on historical trends with a reduced linkage to current priorities and risks	• Proactive asset and integrity management • Safety enhancements and capital projects managed in line with regular everyday activities • Interaction with regulatory authorities based on a current view of systemic risks and actual performance efficiency
Risk-based integrity and asset management	• Asset, system, and consumer data are kept in disparate legacy databases • No formal asset management standards are enforced • Multi-annual investment planning and budgeting • Limited linkage between integrity management and work prioritisation	• Asset, system, and consumer data are validated and kept in enterprise systems/data warehouses • Strategic (annual and quarterly) and tactical (monthly and weekly) asset and work planning cycles are introduced • Analytics and risk modelling linked with monitoring technology and enterprise asset management systems to enable dynamic work identification and prioritisation
Efficient, smart-tech-enabled consumers operations	• Leak survey, corrosion and other inspection performed once every 3–5 years using traditional technologies and approaches • Low degree of system control and automation • Decentralised field and district operational model • Limited utility interaction with consumers “beyond gas meter”	• Frequent inspection and continuous monitoring of asset condition enabled by mobile technology and smart sensors • SCADA connected to a wider array of remote-control valves, automated shut-off valves and sensors with real-time system visualization at a common control centre • Centralised field and district operation model • Utilities provide a wider spectrum of services, including 3rd party vendors and partners, with greater consumer involvement

Source: *PwC*

However, in addition to three key evolution factors listed above, one more factor should be mentioned that most likely will have a significant impact on development trends of the SGD: information privacy. The requirements for the protection of personal data in the EU Member States derive from Regulation (EU) 2016/679 of the European Parliament and of the Council of 27 April 2016 on the protection of natural persons with regard to the processing of personal data and on the free movement of such data, and repealing Directive 95/46/EC (General Data Protection Regulation) [24], which Latvia enforced by the Personal Data Processing Law. It, inter alia, provides that SSOs, as data controllers or processors, must also guarantee data security of the smart metering system and energy consumers [25].

Current data protection strategies are built around a notion that the communication network used in the SGD should be private to ensure total consumer and utility data security. Even when a communication network is private, but shared among different service providers, it is critically important that security firewalls are impenetrable and the system can handle ever-growing use.

3.2. Smart Gas Metering and its Role in Creation of the SGD

Smart gas metering is one of the crucial elements of the SGD as it provides the possibility of uninterrupted, bidirectional data communication in near real-time between consumers and the distribution system operator (hereinafter – DSO) without human intervention [26]. It means that there is no need to send a technician to read gas meters at the consumers' residences or businesses, and therefore expenses of the system management are significantly reduced. Data exchange from the smart gas meter to the central system can be wireless or conducted via fixed wired connections. Wireless communications include cellular communications, Wi-Fi, wireless ad hoc networks over Wi-Fi, wireless mesh networks, low power long-range wireless etc. Wireless mesh networks are currently one of the most reliable and cost-effective IoT connectivity solutions available for a wide range of smart metering applications [27].

Smart gas meters allow for better measurement of energy use, and therefore provide greater opportunities to manage energy demand and improve utilisation of the energy system as well. If smart meters are not deployed, the energy transition and GHG reduction will be more expensive, less supportive of the RE generation, and less well co-ordinated. Without or with very limited smart metering in the EU, CO_2 reduction in Europe's gas sector will be slower and risks of limited participation of the natural gas and RGs in smart energy system development – much higher [28].

The introduction of smart metering in the EU Member States have different timing. In comparison with smart electricity metering, the deployment of smart natural gas meters was and still is much slower. However, benefits of the smart metering system in the natural gas sector are obvious: it not only contributes to more efficient energy use, but also significantly optimises the management of the natural gas supply system and collection, analysis and archiving of data [29], [30].

It is expected that by the end of 2020, the EU countries would invest around EUR 45 billion in installation of around 45 million smart natural gas meters and almost 200 million smart electricity meters. As a result, around 40 % of the natural gas consumers and 75 % of electricity consumers in the EU will use smart electricity and gas metering devices in their households, businesses or public buildings. In most EU Member States, full replacement of mechanical electricity meters has already been introduced or is planned for next 3–5 years, but the use of smart natural gas metering in all segments of consumption is expected in just a few countries, for example, Italy and Finland [30]–[32].

Smart natural gas metering meets requirements for fast and accurate collection, analysis and archiving of the natural gas consumption data, as well as provides opportunities for SSOs to perform more effective evaluation and planning of the natural gas supply system development in various regions of Latvia and other EU Member States. It may also contribute to the achievement of energy efficiency and system security targets [33], [34], which ensure sustainable economic development and prevention of further climate change. Moreover, with the introduction of SGD, costs for smart metering and data processing, archiving and storage are expected to decrease at a rate of approximately 7 % per year.

There is a wide range of smart natural gas meters in use in the EU, which all could be integrated into the smart energy systems

and therefore – SGD. Diaphragm or membrane natural gas meters, which can also be equipped with a data transmission module, are mostly used for a low natural gas flow. In cases where natural gas has to be supplied to a small industrial enterprise or merchant, rotary natural gas meters are preferred. Turbine gas meters are designed to supply natural gas to industrial consumers at a massive, steady flow regime. However, under non-uniform load conditions, turbine meters generate metering errors [35]. Ideally, turbine meters should operate under stable and constant conditions of the natural gas flow in order to avoid pulsations and thus metering inaccuracies. If the flow of natural gas changes or is stopped altogether, the mechanism will continue to rotate for some time; thus, the metering inaccuracies are almost inevitable [36]. The effect of flow disturbances on the readings of the natural gas meter shall not exceed 1/3 of the maximum permissible error of metering instrument of a particular type and technological design.

Diaphragm natural gas meters are used in Latvia up to G25 level because other types of the natural gas meters with a higher performance rate have rather large dimensions and lower accuracy. For example, at times of pulsation of turbine natural gas meters, the inertia of the turbine wheel and subsequent metering error may occur during on and off mode [37].

Ultrasonic and microthermal natural gas meters are an alternative to diaphragm, rotary and turbine natural gas meters. They are used when exclusively high measurement accuracy is required [38]. Microthermal meters can keep an accurate metering rate even at very low initial flows. If correct functioning of diaphragm natural gas meters largely depends on the temperature and pressure, which can be seriously jeopardised without temperature and pressure correction, microthermal meters adjust metering specification to these factors automatically [30]. In contrary to diaphragm natural gas meters, the membranes of which may lose their elasticity over time, microthermal meters do not have moving parts that are subject to wear and tear and can affect the accuracy of metering.

In absence of strict requirements for the choice of technical equipment and software, there is a situation where different data reading systems with different makeup and functionality coexist in the different EU Member States. At some extent it hinders effective, comprehensive development of the SGD. There are also no requirements set for external power supply to smart meters in high gas consumption facilities, where big amounts of data need to be read and transmitted several times a day [30].

In the Latvian natural gas distribution system about 85 % of all consumption data are automatically processed. Data transmission is carried out via GSM communication system by inserting a SIM card into the data transmission device. Around 3,100 pressure and temperature correctors have been installed, of which 510 are equipped with telemetry. According to technical and functional parameters, uniform requirements for the smart meters for natural gas in Latvia have not been determined yet. However, Section 16, Paragraph four of the Energy Efficiency Law (hereafter – EEL) allows the system operator, taking into account the needs and potential benefits of the energy consumers, to determine the minimum functions of a smart commercial metering device, including the possibility to obtain information on actual energy consumption in a specific period of time. The EEL also stipulates that the system operator, when installing a smart commercial metering device, must provide energy consumers with information on the possibilities of

meter management and energy consumption monitoring [39].

The importance of smart metering in the SGD is also determined by the detection and classification of the so-called bad data, which can be represented both by missing data or unusual information exchange patterns caused by unplanned events or failing data collection, communication or entry. As more and more information is fed into the system from different points of origin, the likelihood that mistakes will occur automatically increases. Bad data detection can be divided into probabilistic, statistical, and machine learning methods [40], and all are applicable to the smart energy systems and in part – to the SGD.

4. THE USE OF RGS AND RECONSTRUCTION OF DISTRIBUTION SYSTEM

4.1. RGs as Part of SGD

Increasing sustainability and carbon neutrality of the natural gas infrastructure all over the EU means growing presence of RGs in the natural gas sector. Here biomethane stands out as one of the most promising RGs to be blend with natural gas in large volumes, which can be done in a relatively short period of time [41]. Biomethane is flexible and easily storable fuel that can be used wherever natural gas grids exist without significant improvements to any parts of the natural gas transportation and distribution networks. In those EU regions where a natural gas grid already exists, there is a system suitable for the distribution of biomethane as well. It can be used as a direct substitute for natural gas and as fuel in heating, transport and electricity generation since it has the same properties as natural gas – achieving methane content levels greater than 96 % [42]. However, this methane content level benchmark is not legally or technically binding to all the EU Member States, as they can make their own decisions on how pure biomethane must be in terms of methane content to be injected into the grid [16].

More active use of RGs – mostly, biomethane and hydrogen – and their injection into natural gas distribution grids are important elements in the creation of the SGD. The SGD in principle is meant to be a primary recipient of these injections, as for the natural gas transport infrastructure, much higher injection pressure regimes are required. In Germany that is one of Europe's pioneers in the RG injection into the natural gas grids, several projects were carried out already in the mid-2010s, with biomethane facilities connected to the natural gas transport, instead of the distribution network. However, it must be pointed out that facilities connected directly at the natural gas transport level presented rather significant biomethane production capacities and were able to maintain the required high-pressure injection regime. For instance, it relates to Bioenergie Park in Güstrow, which provided the natural gas transportation grid with biomethane input at a maximum rate of up to 5000 m^3/h [43].

In Latvia, the injection of biomethane is also legally allowed in both natural gas transmission and distribution networks. Paragraphs 6 and 7 of Regulation of the Cabinet of Ministers No.650 "Requirements for the Injection and Transport of Biomethane and Gaseous Liquefied Natural

Gas in the Natural Gas Transmission and Distribution System" states that if biomethane is injected into the natural gas transmission system, where a minimum pressure at the moment is 25 bar, but most likely will be risen to 50 bar in the nearest future, its pressure must not exceed the actual pressure of the system by more than 5 bar. On the other hand, if biomethane is injected into the natural gas distribution system, its operating pressure must exceed the pressure of the system by not more than 10 % of the actual pressure at the connection point [44], [16].

It means that in future, when actual biomethane injections into the Latvian natural gas distribution network begins, the grid automation will need to address not only existing elements of the system in use today, but also those that will come online with grid introduction of the RG.

4.2. Modernisation of the Natural Gas Distribution System in Latvia

Successful implementation of the SGD in Europe as a whole and in Latvia in particular is hardly possible without complex, strategic enhancement of current natural gas distribution systems. DSOs have to modernise grids in order to preserve their technical capabilities and to make them more suitable for integration of new automated elements. Given the monopolistic status of many European gas DSOs, in future it will be necessary to couple their traditional regulated service functions with new market and systemic demands. The gradual natural gas distribution automation is about improved efficiency in grid operation, reducing operation costs and increasing grid reliability by introduction of a higher degree flexibility and autonomy.

In case of Latvia, the implementation of at least several elements of the SGD is fully up to the DSO JSC Gaso that, since its creation in late 2017, owns and manages all the natural gas distribution infrastructure in the country [45]. The major part of the natural gas distribution infrastructure in Latvia was built more than fifty years ago. Many of its elements are physically and morally outdated, so planned replacements are unavoidable. Complex repairs are not always possible without interruption of natural gas supply to consumers, but reduction of interruption duration, along with the modernisation of the natural gas supply system itself, is one of the strategic priorities defined by the Latvian gas DSO.

Both in the case of natural gas and electricity, several technical references are used to determine the level of system functionality, which characterise the number and duration of supply disruptions, as well as renewal of supply after unplanned disruptions. In 2019, the number of the natural gas supply interruptions (SAIFI) and duration (SAIDI) per consumer in the natural gas distribution system was 0.48 times and 56 minutes, respectively. In total, unplanned natural gas supply interruptions occurred 425 times. Additionally, the time for renewal of natural gas supply after unplanned interruptions (CAIDI) in 2019 corresponded to 88 minutes or 1.5 hours [46].

By comparing the information on the natural gas distribution SAIDI indicators of the Finnish, German, Lithuanian, Austrian and Latvian natural gas DSOs, it can be concluded that the performance of the Latvian DSO almost fully correlates with them. On average, during scheduled repairs, the natural gas supply outages last from 4 to 6 hours, and they are implemented on workdays – when the economically active part of the society is absent [46]. In very rare

situations, while carrying out large-scale replacement of the technological equipment or reconstruction of the major system elements, it is necessary to disconnect customers for several days or even a week. However, the proportion of such works corresponds only to 5 % of all planned repairs carried out by JSC Gaso [47].

Annual investments in repairs and modernisation of the natural gas distribution system for next five years are equal to about EUR 5.5 million. These funds mainly go to activities, which, inter alia, will be of the utmost importance for further system automation and digitalisation as well, and they are: stabilisation of the natural gas network, reconstruction of regulation equipment, water seals, syphons and improvement of cathodic protection of natural gas pipelines. These investments, without which it is impossible to ensure the secure and stable development of natural gas supply in Latvia in a mid- and long-term perspective, fall into six main categories listed in Table 4 in descending order.

Table 4. Average Investments of Natural Gas Distribution System Modernisation (by category, in EUR per year)

Reconstruction of pipelines (cross-connection (looping), stabilisation, security of supply)	1.950.000
Reconstruction of gas regulation points	1.145.000
Shutting-off device replacement programme	800.000
Water seal and syphon replacement programme	350.000
Renovation of gas inlets of buildings	950.000
Improvement of cathodic protection	300.000
Total	5.495.000

Source: JSC Gaso

As it has been mentioned before, many elements of the Latvian natural gas distribution system are outdated, so their replacement needs to be carefully planned and implemented step by step. For instance, system looping significantly reduces risks for the stable operation of all types of natural gas distribution pipelines. It ensures that pressure stabilisation is achieved in the loaded sections of a system, and natural gas supplies from several directions can be carried out. There are also additional possibilities of the natural gas flow variation by using independent natural gas supply sources, when repair or reconstruction of individual gas pipeline sections is required, or in case of emergency. As a result, the level of security of the natural gas supply and system accessibility for new natural gas consumers increase significantly.

Works are also underway on the reconstruction of the equipment ensuring the stability of the natural gas supply itself, namely, gas control points (hereinafter – GCPs). At present, there are about 180 GCPs located in buildings in Latvia and several thousand cabinet-type GCPs. Every year, 5–6 GCPs in buildings, as well as several dozen cabinet-type GCPs are renovated.

During routine maintenance of GCPs, various technical problems and defects are often identified, and many of them are eliminated without delay. On the other hand, problems, which cannot be solved immediately, are included in capital investment and reconstruction programmes of JSC Gaso. The urgency of repairs mainly depends on the nature of defects, as they can vary from damaged fence to significant malfunctions in the major components of equipment, which

require immediate replacement of damaged parts or even a complete reconstruction of GCPs. Where technically possible, GCPs are replaced by cabinet-type GCPs. It helps optimise the system and make it more compact: the GCP in a building normally takes up a large amount of space, but a cabinet-type GCP does not require more than a few square meters. In addition, both GCP and cabinet-type GCP can be equipped with telemetry, which allow obtaining data on the operation of the natural gas distribution network, thus increasing its operational safety and ensuring timely detection of non-standard situations and accidents.

During routine inspections of the shut-off devices (valves) located in wells or on the ground surface, various types of damage are detected regularly. Many of them can be immediately eliminated. But, if it is not possible, decisions are made to replace or liquidate the shut-off devices, by including these activities in the corresponding capital investment programmes [47].

Dismantling of the water seal and syphon installed during the Soviet era is also carried out gradually. Water seals of a low-pressure gas supply systems are used to interrupt the supply of natural gas, but syphons are designed to eliminate the liquid in gas pipelines. The usage of water seals is relatively safe, but their exploitation is rather complicated – during the shutting-off process water can enter the system, which can interfere with the normal operation of the natural gas supply. In addition, maintenance of a water seal is quite expensive in comparison with other shut-off technologies, and it cannot be automated. Syphons are mainly built in the former liquefied gas systems, and the necessity to preserve them is rarely justified. To some extent water seals and syphons pose one of the main hazards in terms of safety and integrity of the distribution pipeline system, because they are up to sixty years old, manufactured in workshops, their welds are not radiated and they are located in densely populated areas – mainly, in the courtyards of multi-storey apartment buildings.

In context of developing SGD, one of the future priorities for the European natural gas DSOs, including JSC Gaso, would be a necessity of further automation of the system, starting from consumption side and smart metering, and ending with the most robust parts and equipment used in the natural gas distribution in Latvia. It would allow following the actual trends of the DSO activities in Europe, improving sustainability of the system and optimising future inspection and maintenance costs.

5. CONCLUSIONS

The importance of gaseous fuels and the SGD in the future production, transportation and use of energy in the EU should not be underestimated. Gas grids will play one of the central roles in the overall shaping of the energy strategy thanks to their flexibility and compatibility with RE, including such RGs as biomethane and hydrogen. Storage abilities of the natural gas network, as well as RG and P2G technologies, will help solve many problems to attain to future energy efficiency in a sustainable way.

Although the SGD is not the first priority in the European debate concerning energy efficiency and development of the smart energy systems, the natural gas industry has been an active promoter of the synergic potential of the natural gas sector, and it refers to the gas distribution infrastructure, too. Furthermore, the existing natu-

ral gas infrastructure allows implementing cutting-edge innovative solutions for wider use of RGs. For instance, P2G shows that SGD can be used to store and transport the excess production of RE. RGs have been injected into the existing natural gas grids throughout the EU for more than ten years, and the potential for growth in this area is very large. Even in Latvia, it is estimated that biogas production potential is very substantial, including biomethane yearly production of about 300 gigawatt hours [48].

Natural gas networks have the ability to store a large amount of energy without additional storage improvement investments, and thus are much more flexible than electricity networks.

The potential of the SGD in Latvia is significant, as many elements of the system are currently digitalised, remotely controlled and inspected, so their integration into a single network, with gradual widening of its smart segment, resonates well not only with a universal need for modernisation, but also with investment in reasonable enhancement of flexibility, sustainability and future competitiveness of the existing natural gas distribution infrastructure.

ACKNOWLEDGEMENTS

The research has been supported by the National Research Programme, project "Trends, Challenges and Solutions of Latvian Gas Infrastructure Development" (LAGAS) (No. VPP-EM-INFRA-2018/1-0003).

REFERENCES

1. International Gas Union. (2020). *Global Gas Report 2020*. [online]. [accessed 14 November 2020]. Available at https://ceenergynews.com/reports/igu-global-gas-report-2020/
2. Stern, J. (2017). *The Future of Gas in Decarbonising European Energy Markets: The Need for a New Approach*. OIES Paper: NG 116.
3. Eurostat. (2018). *Natural gas supply statistics*. [Online]. [Accessed: 8 October 2020]. Available at https://ec.europa.eu/eurostat/statistics-explained/index.php?title=Natural_gas_supply_statistics&oldid=401136
4. Savickis, J., Zeltins, N. & Jansons, L. (2019). Synergy between the Natural Gas and RES in Enhancement of Security of Energy Supply in the Baltic Countries (problem statement): The Latvian Perspective. *Latvian Journal of Physics and Technical Sciences, 56* (6), 17–32. DOI: 10.2478/lpts-2019-0032.
5. Savickis, J., Zeltins, N., Kalvītis, A., & Ščerbickis, I. (2018). Natural Gas Development Prospects in the World, Europe, in the Baltic and Latvia. *Energy and World Special Edition* (dedicated to the 4th World Latvian Scientists' Congress, June 2018, Riga).
6. Verdolini, E., Vona, F., & Popp, D. (2018). Bridging the Gap: Do Fast Reacting Fossil Technologies Facilitate Renewable Energy Diffusion? *Energy Policy, 116,* 242–256.
7. European Gas Hub. (2019). *Lowest European gas prices in 10 years*. [online]. [accessed 5 November 2020]. Available at https://www.europeangashub.com/lowest-european-gas-prices-in-10-years.html
8. Interactive CO_2 pricing data hub Embler. [online]. [accessed 12 November 2020]. Available at https://ember-climate.org/data/carbon-price-viewer/
9. ECRB. (2019). *Monitoring Report on the Functioning of Gas and Electricity Retail Markets in the Energy Community in 2018*.

10. Eurostat. (n.d.). *Gas prices by type of user*. [online]. [accessed 3 November 2020]. Available at https://ec.europa.eu/eurostat/web/products-datasets/-/ten00118
11. Statista. (n.d.). *Share of natural gas imported to the European Union (EU) from Russia from 2010 to 2018 (as percentage of total extra-EU natural gas imports)*. [online]. [accessed 22 November 2020]. Available at https://www.statista.com/statistics/1021735/share-russian-gas-imports-eu/
12. European Environment Agency. (2018). *Air quality in Europe – 2018 Report*. [online]. [accessed 1 November 2020]. Available at https://www.eea.europa.eu/publications/air-quality-in-europe-2018
13. International Energy Agency. (2019). *The Role of gas in today's energy transitions*. World Energy Outlook special report. [online]. [accessed 4 October 2020]. Available at https://webstore.iea.org/login?ReturnUrl=%2fdownload%2fdirect%2f2819%3ffileName%3dTheRoleofGas.pdf&fileName=TheRoleofGas.pdf
14. PwC. (2015). *Realizing the benefits of smart gas distribution*. PwC series: The promise and potential of smart gas distribution. [online]. [accessed 20 November 2020]. Available at https://www.pwc.se/sv/energi/assets/realizing-the-benefits-of-smart-gas-distribution.pdf
15. Lund, H., Østergaard, P.A., Connolly, D., & Mathiesen, B.V. (2017). Smart Energy and Smart Energy Systems, *Energy*, *137*, 556–565. DOI 10.1016/j.energy.2017.05.123
16. Savickis, J., Zemite, L., Zeltins, N., Bode, I., Jansons, L., Dzelzitis, E., … & Ansone, A. (2020). The Biomethane Injection into the Natural Gas Networks: The EU's Gas Synergy Path. *Latvian Journal of Physics and Technical Sciences, 57* (4), 34–51. DOI: 10.2478/lpts-2020-0020.
17. Smart Energy Networks. (2015). *Vision for smart energy in Denmark: Research, development and demonstration.* [online]. [accessed 14 November 2020]. Available at http://www.smartenergynetworks.dk/uploads/3/9/5/5/39555879/vision_for_smart_energy_in_denmark.pdf
18. Miller, W.J. (2017) Internet of Things (IoT) for smart energy systems. In Gabbar, H.A. (ed.) *Smart Energy Grid Engineering*. [online]. [accessed 2 November 2020]. Available at https://www.sciencedirect.com/science/article/pii/B9780128053430000115
19. Staffell, I., Scamman, D., Velazquez Abad A., Balcombe, P., Dodds, P., Ekins, P., … & Ward, K. (2018). The Role of Hydrogen and Fuel Cells in the Global Energy System. *Energy & Environmental Science*, *12* (2): 463–491. DOI:10.1039/C8EE01157E
20. Bouhafs, F., Mackay, M., & Merabti, M. (2014). *Communication challenges and solutions in the smart grid*. Springer
21. Sioshansi, F. (ed.). (2019). *Consumer, prosumer, prosumager: How service innovations will disrupt the utility business model.* Academic Press.
22. Smart Energy. (2015). *IGU World Gas Congress 2015*. Grid aspects related to Gas.
23. Sayed, K., & Gabbar, H.A. (2017). SCADA and smart energy grid control automation. In Gabbar, H. A. (ed.) *Smart Energy Grid Engineering*. 10.1016/B978-0-12-805343-0.00018-8
24. Regulation (EU) 2016/679 of the European Parliament and of the Council of 27 April 2016 on the protection of natural persons with regard to the processing of personal data and on the free movement of such data, and repealing Directive 95/46/EC (General Data Protection Regulation). [online]. [accessed 20 October 2020]. Available at https://eur-lex.europa.eu/eli/reg/2016/679/oj
25. Fizisko personu datu apstrādes likums. (2018). [online]. [accessed 6 October 2020]. Available at https://likumi.lv/ta/id/300099-fizisko-personu-datu-apstrades-likums
26. ERRA. (2010). *Regulatory aspects of smart metering*. [online]. [accessed 5 November 2020]. Available at https://erranet.org/wpcontent/uploads/2016/03/KEMA_Issue_Paper_Smart_Metering_FINAL_eng.pdf
27. Geelen, D., van Kempen, G., van Hoogstraten, F., & Liotta A. (2012). A wireless mesh communication protocol for smart-metering. *International*

Conference on Computing, Networking and Communications (ICNC), 30 January–2 February 2012, Maui, HI, USA. DOI: 10.1109/ICCNC.2012.6167440

28. Delta Energy and Environment. (2019). *Smart meter benefits. Role of smart meters in responding to climate change.* [online]. [accessed 9 November 2020]. Available at https://www.smartenergygb.org/en/resources/press-centre/press-releases-folder/delta-ee-carbon-savings
29. Toratti, J. (2020). *Appraising the economics of smart meters: Costs and benefits*. London: Routledge.
30. Savickis, J., Zemite, L., Bode, I., & Jansons. L. (2020). Natural Gas Metering and its Accuracy in the Smart Gas Supply Systems. *Latvian Journal of Physics and Technical Sciences, 57* (5), 39–50. DOI: 10.2478/lpts-2020-0026.
31. Report from the Commission. *Benchmarking Smart Metering Deployment in the EU-27 with a Focus on Electricity* /* COM/2014/0356 final */ [online]. [accessed 1 November 2020]. Available at https://eur-lex.europa.eu/legal-content/GA/TXT/?uri=COM%3A2014%3A356%3AFIN
32. Bianchini, A., Saccani, C., Guzzini, A., & Pellegrini, M. (2018). *Gas smart metering in Italy: State of the art and analysis of potentials and technical issues*. [online]. [accessed 10 November 2020]. Available at https://www.researchgate.net/publication/330260200_Gas_smart_metering_in_Italy_state_of_the_art_and_analysis_of_potentials_and_technical_issues
33. Zemite, L., Kutjuns, A., Bode, I., Kunickis, M., & Zeltins, N. (2018). Consistency Analysis and Data Consultation of Gas System of Gas-Electricity Network of Latvia. *Latvian Journal of Physics and Technical Sciences, 55* (1), 22–34. DOI: 10.2478/lpts-2018-0003.
34. Koposovs, A., Bode, I., Zemite, L., Dzelzitis, E., Odineca, T., Ansone, A., … & Jasevics, A. (2019). Optimization of the Selection Method for Reconstruction of Outworn Gas Distribution Pipeline. *Latvian Journal of Physics and Technical Sciences, 56* (5), 33–44. DOI: 10.2478/lpts-2019-0029.
35. Stoltenkampa, P.W., Bergervoetb, J.T.M., Willemsa, J.F.H., van Uitterta, F.M.R., & Hirschberga, A. (2008). Response of Turbine Flow Meters to Acoustic Perturbations. *Journal of Sound and Vibration*, 258–278.
36. Cascetta, F., & Rotondo, G. (2015). Effects of Intermittent Flows on Turbine Gas Meters Accuracy. Second University of Naples, *Italy Measurement, 69*, 280–286.
37. Platais, I., & Graudiņš, P. (2008). *Gāzapgāde. 1.daļa. Ogļūdenražu deggāzes, to īpašības, metroloģija un sadedzināšana*. Rīga: RTU izdevniecība.
38. Homann, K., Reimert, R., & Bernhard, K. (2013). *The gas engineer's dictionary. Supply infrastructure from A to Z.* Germany: DIV Deutscher Industrieverlag GmbH.
39. Energoefektivitātes likums. (2016). [online]. [accessed 11 August 2020]. Available at https://likumi.lv/doc.php?id=280932
40. Hodge, M., & Austin, J. (2004). A Survey of Outlier Detection Methodologies. *Artificial Intelligence Review, 22* (2), 85–126.
41. Outlook for biogas and prospects for organic growth. (2020). [Online]. [Accessed: 6 October 2020]. Available at https://www.euneighbours.eu/sites/default/files/publications/ 202003/Outlook_for_biogas_and_biomethane.pdf
42. European Biogas Association. (n.d.). *EBA's biomethane fact sheet*. [Online]. [Accessed: 22 November 2020]. Available at https://www.europeanbiogas.eu/wp-content/uploads/files/2013/10/eba_biomethane_factsheet.pdf
43. Green Gas Initiative. (2016). *Gas and Gas Infrastructure – the Green Commitment*. Recommendations for curbing climate change: Biomethane, power to gas and gas as fuel in transport [online]. [accessed 1 November 2020]. Available at https://www.greengasinitiative.eu/upload/contenu/greengas_initiative_report_web_2016_1.pdf

44. Ministru kabineta noteikumi Nr. 650. (prot. Nr. 50 5. §) “Prasības biometāna un gāzveida stāvoklī pārvērstas sašķidrinātās dabasgāzes ievadīšanai un transportēšanai dabasgāzes pārvades un sadales sistēmā”. [Online]. [Accessed: 20 October 2020]. Available at: https://likumi.lv/ta/id/285189-prasibas-biometana-un-gazveida-stavokli-parverstas-saskidrinatas-dabasgazes-ievadisanai-un-transportesanai-dabasgazes-parvades-...
45. GASO. [online]. [accessed 20 November 2020]. Available at https://www.gaso.lv/uznemuma-rasanas
46. *Elektroenerģijas un dabasgāzes sadales pakalpojumu kvalitātes pārskats par 2019. gadu* [online]. [accessed 1 November 2020]. Available at https://www.sprk.gov.lv/sites/default/files/editor/ED-Kvalitates-parskats_2019%20(3)_0_0.pdf
47. AS “Gaso”. (2018). *Piecu gadu investīciju (attīstības) programma*.
48. Bethers, J. (2020). *Enerģētikas sektora izaicinājumi ceļā uz klimata neitralitāti 2030/2050*. Conference presentation.

sciendo

LATVIAN JOURNAL OF PHYSICS
AND TECHNICAL SCIENCES
2020, N 6

DOI: 10.2478/lpts-2020-0032

MEASURES TO ACHIEVE THE ENERGY EFFICIENCY IMPROVEMENT TARGETS IN THE MULTI-APARTMENT RESIDENTIAL SECTOR

M. Upitis[1*], I. Amolina[2], I. Geipele[2], N. Zeltins[3]

[1]JSC "Development Finance Institution Altum"
4 Dome Square, Riga, LV-1050, Latvia
E-mail: martins.upitis@altum.lv
[2]Riga Technical University,
Institute of Civil Engineering and Real Estate Economics,
6 Kalnciema Str., Riga, LV-1048, LATVIA
[3]Riga Technical University, Institute of Power Engineering
12-1 Azenes Str., Riga, LV-1048, LATVIA
*e-mail: martins.upitis@altum.lv

Directive (EU) 2018/2002 of the European Parliament and of the Council amending Directive 2012/27/EU on energy efficiency sets a target of 32.5 % energy efficiency to be achieved by 2030, with a possible upward revision in 2023. The directive also stipulates that the obligation to achieve annual energy savings must continue to be met after 2020. In addition, a revised directive on the energy performance of buildings was adopted in May 2018. It includes measures to speed up the renovation of buildings and the transition to more energy-efficient systems, as well as to improve the energy efficiency of new buildings, thus using smart energy management systems [1].

Buildings consume the most energy and have the greatest energy saving potential. They are therefore crucial to achieving the European Union's energy saving targets. The EU allocated around 14 billion EUR to improve the energy efficiency of buildings in the period of 2014–2020, of which 4.6 billion EUR was intended for residential buildings. In addition, the Member States have earmarked 5.4 billion EUR of public co-financing for the improvement of all types of buildings, of which around 2 billion EUR is allocated to residential buildings.

Multi-apartment residential buildings in Latvia are in a technically unsatisfactory condition. In Latvia, the service life of multi-apartment residential buildings has been artificially extended. In addition, there is also the problem of reduced construction quality. Housing problems affect all layers of society, but they are most acute for low- and middle-income people.

The aim of the research is to study, using the co-financing of the European Union Structural Funds, the activities performed during the renovation process of multi-apartment residential buildings in Latvia and to identify the shortcomings.
Keywords: *Construction quality, energy efficiency, renovation of residential houses.*

1. INTRODUCTION

In Latvia, the main volume of multi-apartment buildings up to 75 % is made up of standard residential houses built in the period from 1946 to 1993. The average specific heat consumption for heating of these apartment buildings is 157 KWh/m^2 per year (Ministry of Economics). The results of multi-apartment building renovation projects implemented in European countries and Latvia demonstrate that by performing complex insulation it is possible to reduce heat energy consumption for heating by 40–60 % of the initial consumption [2].

Compliance with the established norms on energy efficiency of buildings and binding state priorities are topical for the national economy:

1. A comprehensive increase in energy efficiency has become a cornerstone of a country's energy independence.
2. Reduction of harmful CO_2 emissions.
3. Improving the energy efficiency of the manufacturing and service sectors is a matter of both competitiveness and the quality of work and the environment.
4. Directive 2002/91/EC of the European Parliament and of the Council of 16 December 2002 on the energy performance of buildings, which is adopted by the Republic of Latvia, envisages an increase in energy efficiency to meet the Kyoto Protocol aimed to reduce CO_2 emissions.

These requirements ensure sustainable economic development and prevention of further climate change [3].

Energy efficiency has gained a lot of prominence in recent debates on urban sustainability and housing policy due to its potential consequences for climate change. At the local, national and also international level, there are numerous initiatives to promote energy savings and the use of renewable energy to reduce the environmental burden. There is a lot of literature on energy savings and other forms of energy efficiency in housing [4].

The topicality of the research is determined by several aspects:

1. It is important for the owners of multi-apartment residential buildings to reduce the costs of heat energy. There is a human natural tendency to live rationally and save heat energy and other resources, if one has to pay for them; thus, it leads to economical use of energy.
2. In the period from 1955 to 1992, reinforced concrete structures were widely used in construction. The construction of buildings of this period is characterised by high specific energy consumption and low heat resistance of building envelopes.
3. Multi-apartment residential buildings constructed in the 50s and 60s are approaching the end of the normative service life; depreciation of engineering services of buildings is 70–100 %.
4. During the European Union funds planning period, apartment owners in multi-apartment buildings have the oppor-

tunity to receive co-financing for the implementation of energy efficiency improvement measures.

The goal of the research is to study the implementation of energy efficiency measures in multi-apartment residential buildings and the achieved indicators using the co-financing of the European Union Structural Funds.

To achieve the goal, the following objectives are set: 1) to study scientific articles on the chosen topic; 2) to find out the main achievable indicators in the implementation of the programme; 3) to find out the tools to make sure of the quality of construction work.

The subject of the research is energy efficiency measures for multi-apartment residential buildings, and the object of the research – multi-apartment residential buildings.

In the course of literature analysis, the authors have used topical articles of the Web of Science and Scopus scientific databases and unpublished information from state-owned development finance institute Altum.

2. THE NATURE OF ENERGY EFFICIENCY

The explanation of the concept of energy efficiency should be considered not only in Latvian, but also in the European Union (hereinafter – the EU) and global context. Definitions of energy and related concepts are provided both in Directive 2012/27/EU of the European Parliament and of the Council of 25 October 2012 on energy efficiency, amending Directives 2009/125/EC and 2010/30/EU and repealing Directives 2004/8/EC and 2006/32/EC, and in regulatory enactments of the Republic of Latvia related to the energy sector.

Article 2 of Directive 2012/27/EU of the European Parliament and of the Council provides the following definition: "energy efficiency means the ratio of output of performance, service, goods or energy, to input of energy" [5].

Article 2 of Directive 2010/31/EU of the European Parliament and of the Council provides the following definition: "energy performance of a building means the calculated or measured amount of energy needed to meet the energy demand associated with a typical use of the building, which includes, inter alia, energy used for heating, cooling, ventilation, hot water and lighting" [6].

According to the Law on the Energy Performance of Buildings and the explanation of the Ministry of Economics of the Republic of Latvia, energy performance of a building is the relative amount of energy, which characterises the necessary energy consumption for the supply of heating, ventilation, cooling, lighting and hot water in the typical operating conditions of a specific type of building. The energy performance of a building is expressed in kilowatt hours per square meter per year (kWh/m2 per year) [7].

In the course of the examination of the energy efficiency concept, the authors conclude that energy efficiency can be characterised as a change in values, which can manifest itself as both a reduction in energy consumption and an increase in the level of productivity. Energy efficiency is understood as the reduction in the amount of energy consumed – the difference between the identified energy consumption before the implementation of energy efficiency solutions and the calculated or determined energy consumption after the implementa-

tion of energy efficiency measures.

Electricity consumption in energy efficiency projects is also important. Since the European Commission has suggested that all the EU Member States should discontinue season-dictated time changing, the economically best-grounded solution in terms of electricity consumption is the scenario where country chooses staying at summer time and the Nord Pool countries – at winter time. In the construction sector, summer time has a positive impact – considering the relatively short building season [8].

The concept of smart grid has received significant attention in recent times due to climate change sustainability, uses requirements of higher supply reliability and quality [9].

Most of the urban housing stock in Latvia as well as in the major part of EU cities consists of multi-storey apartment buildings. The improvement in energy efficiency of these buildings is the key priority in many countries. However, unclassified buildings have a significant potential for the application of innovative energy efficiency measures [10].

Although in littoral regions of the Baltic Sea in Latvia multi-storey residential buildings with a large number of apartment owners are not dominant, different opinions of the owners about the implementation of energy efficient solutions and their financial capacity impede the energy efficient process management. Often, apartment owners are not well informed and aware of the issues related to energy efficient solutions and energy efficient process, as well as of the management of joint ownership of houses; therefore, they passively take part in the decision-making process [11].

The EU Member States are in the process of implementing energy rating procedures for buildings. For non-domestic buildings in particular, devising a robust and cost effective energy rating method is not a simple task. The situation becomes more complicated where countries do not have a tradition of performing energy calculations or undertaking energy measurements in buildings [12].

Buildings, which form the accumulated wealth of a country during a long time and are frequently the largest asset of each country, should be renovated, considering the benefit as well of the timely renewal of worn out building elements.

For example, the Energy Efficiency Housing Pilot Project in Lithuania, which was initiated by the World Bank and directed to the renovation of residential houses and educational institution buildings, has shown that at present, residential and public buildings built between 1960 and 1980 face two problems – an inefficient heat consumption and a deterioration of building elements and engineering systems. This in turn results in conditions inside buildings that do not comply with up-to-date requirements of comfort and safety [13].

In general, it can be concluded that the nature of energy efficiency and related activities in the process of renovation of multi-apartment buildings should be implemented using a model, which will increase the efficiency, comfort and exterior of a dwelling. Measures should be taken on the basis of high level energy audit results, determining the main problems, identifying the main causes of heat loss, during the renovation of the dwelling focusing on the main problems, which result in high heat loss from the dwelling, the main defects in the structures, the renovation of which will increase the life cycle of residential buildings.

3. DISCUSSION AND RESULTS

In Latvia, a large part of multi-apartment residential buildings was constructed in the period from 1946 to 1993 [14]. These buildings are characterised by high wear and tear of building structures and engineering systems, as well as low energy efficiency. Since 2016, the support of the EU structural funds in the amount of 156 million EUR has been available in the country to renovate multi-apartment buildings (85 % of the EU structural funds, 15 % of state funding). It is envisaged that this funding will be enough for about 1,030 multi-apartment buildings. The implementer of the financial instrument in this period is JSC "Development Finance Institution Altum" [15]. Support in this programme is provided in the form of grants, loans, guarantees and advice (DME programme). The specific objective of the programme is to promote energy efficiency and the use of smart energy management and renewable energy in multi-apartment residential buildings. To receive the EU support within this programme, the heating consumption of a residential building after the performance of works shall not exceed 90 kWh/m² per calendar year.

The average heat consumption for heating of multi-apartment residential buildings submitted to the DME programme is 155 kWh/m²; information on the projects submitted to the DME programme until 15 October 2018 is summarised in Figs. 1 and 2.

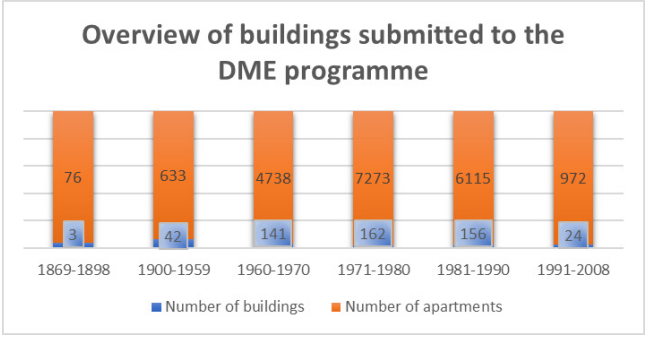

Fig. 1. The number of multi-apartment residential buildings and households (apartments) in the DME programme until 12 July 2020 (created by the authors using Altum information).

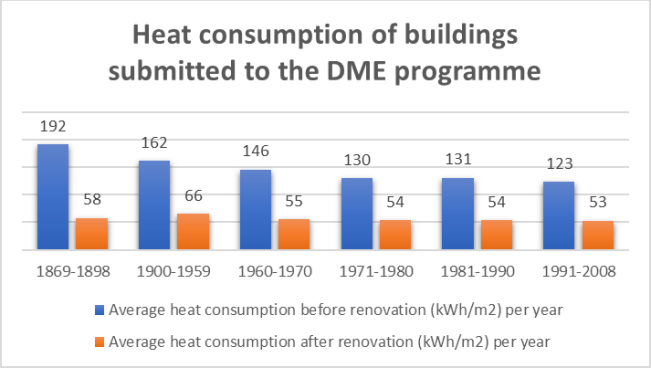

Fig. 2. Summary of current and planned average heat consumption per year of multi-apartment residential buildings before and after renovation of buildings (created by the authors using [14–16]).

There are 38.6 thousand multi-apartment residential buildings (three- or more apartment buildings) in Latvia with a total area of 50.4 million m² (1305 m² per building) [14]. It is possible to perform cost-effective renovation of 60 % to 70 %, or about 25 thousand apartment buildings with a total area of 38 million m². A small part (3 % of the total number of houses – 741 buildings) has been renovated in the EU funds programming period of 2007–2013, while the buildings built after 2003 (approximately 3 % of the total number of buildings) are relatively energy efficient, with low energy consumption. The number of potentially energy efficient renewable buildings in Latvia is approximately 23,500 (94 % of 25,000) with a total area of 30.6 million m².

Latvia has set high targets in the field of energy efficiency. In order to increase the energy efficiency of multi-apartment buildings, a complex approach is required, reaching the specific heat consumption for heating in the amount of 70–90 kWh/m²/year after the renovation of buildings (minimum requirements of the DME programme). To achieve such specific heat consumption, the project must achieve a total heat saving of 85 kWh/m² on average. In turn, in order to achieve such heat energy savings, the investment costs per m² of the total area of the building must be approximately 156 EUR (see Fig. 3 below).

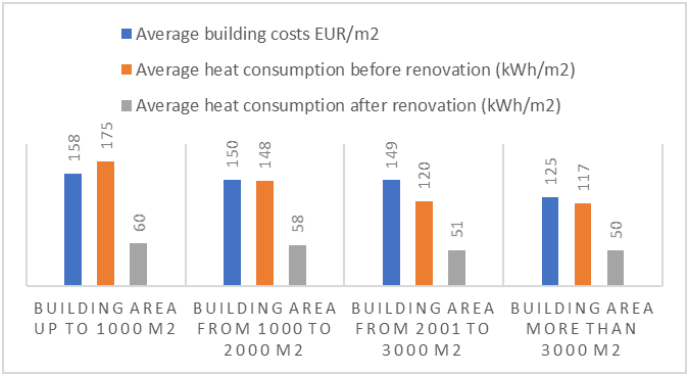

Fig. 3. Costs and heat consumption divided by the total m² of the building (distribution by m², up to 1000, from 1000–2000, from 2001–3000, more than 3000) (created by the authors).

When implementing building renovation works, great emphasis is placed on high-quality technical project documentation, so that there would be as few unforeseen works as possible during the project implementation stage, which could have been foreseen at the design stage but were not performed. In order to qualitatively prepare the DME (energy efficiency of a multi-apartment building) project, the following documents are required:

1. Building energy certificate;
2. Structure technical inspection opinion by a construction specialist;
3. Construction project drawn up by a construction specialist or a building facade confirmation card and work organisation project;
4. Certification card made by a construction specialist for engineering structures;
5. Construction volumes or control estimate.

Works that could provide energy efficiency are determined by the energy certificate of a building. The annex to the certificate indicates what work should be done to improve the overall energy performance of a building.

Usually these works are related to the insulation of the building enclosing structures (building facade, plinth, and roof), basement insulation, attic insulation, replacement of windows and doors both in the apartments and in the staircase. Of course, one cannot forget about the renovation of the building engineering systems (heating and hot water) to ensure the regulation of heating consumption according to the wishes of each resident, so that each consumption can also be accurately accounted for, generally ensuring comfort in apartments.

Evaluating the construction contracts submitted to the DME programme, it has been established that mostly project implementation is not carried out according to the planned plan – Project Time Schedule.

As soon as it is established that deviations are planned and the construction deadlines are not met, it is necessary to amend the contract, including an agreement on the extension of the term of work. Below statistics is provided (see Fig. 4) on how many of the completed projects were on time, how many were not, or whether there was an extension of deadlines.

In order to extend the term of work, the builder needs to submit a substantiated application/letter to the customer and a new time schedule, while the customer draws up an affirmation act and an agreement within the contract. This information is then submitted to Altum, where the legal aspect and the requirements set out in the procurement regulations are assessed.

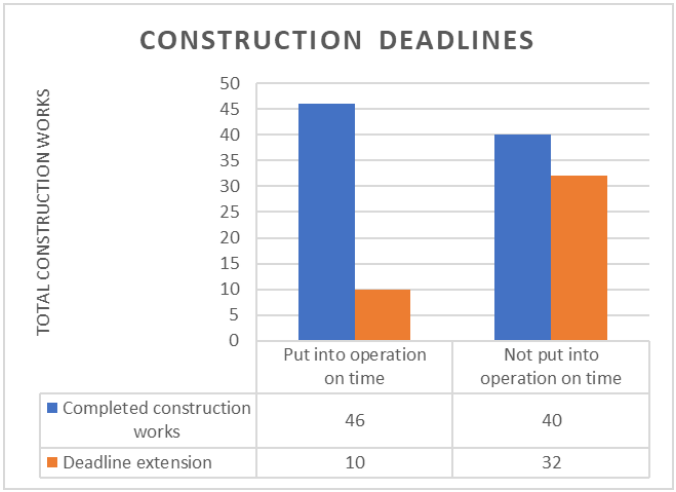

Fig. 4. Terms of the construction contract
(created by the authors using Altum information).

There are several typical trends in the DME programme that recur, where the builder offers relatively short deadlines and is unable to meet them.

Construction works shall be carried out by a construction contractor registered in the Register of Construction Merchants. The supervision of the works is performed by a certified construction contractor, who makes daily entries in the construction work log regarding the performed works and the materials used. According to the construction completion deadlines (see Fig. 5), only 1 out of 30 projects has been completed within the planned deadline.

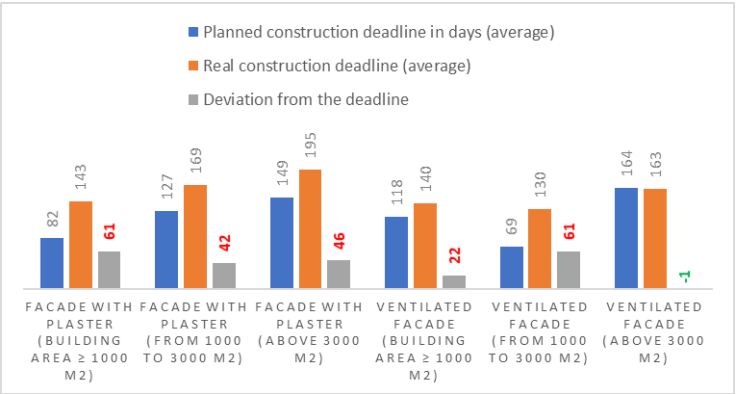

Fig. 5. Division by the planned and actual work execution (created by the authors using Altum information).

Construction companies, implementing DME projects even after several deadline extensions, cannot complete the work within the set deadlines. It is crucial that when concluding contracts in the autumn, but starting work in the spring next year, the entrepreneur faces a shortage of materials or rising material prices, which affect the purchase of materials and construction deadline.

To control the quality of construction work in terms of the energy efficiency of a building, a control tool – thermography with a thermal chamber – is often used. Using the infrared radiation generated by a building, the surface temperature of the structure is determined and plotted in a plane by means of a colour scale. This method allows quickly obtaining visual data on the quality of the work performed and it is not necessary to expose the defect site.

Thermography uses a qualitative test method, i.e., one surface is compared with another or with itself, thus identifying problem areas, but it is not possible to determine the flow of heat through the building surfaces, such as the heat transfer coefficient of a building element or building permeability.

The thermography method is more used in cases when the building envelope is insulated with a plastered facade solution. Another limitation of this test method is that the thermographic survey cannot be performed if the energy efficiency works in a building are carried out at a time when the temperature difference between the indoor and outdoor environment is insufficient to perform a qualitative survey (in summer).

In the DME programme, insulation of enclosing structures with a ventilated facade is used in some objects, which means that there is no direct thermal contact between the main structure of the exterior wall and the facade finishing material; as a result, it is not possible to fix the defect in the main structure. In such cases, in order to determine the quality of the work carried out, it is necessary to perform a building density test or BlowerDoor test.

The BlowerDoor test method works on the principle of creating a pressure difference of 50 Pa between the interior and the exterior of the building, thus determining the amount of outdoor air entering the structures through various leaks. The BlowerDoor tool consists of a calibrated fan air flow measurement and special measuring devices to determine the pressure difference between two measuring environments.

Tables 1 and 2 below summarise the images from the post-monitoring of the site, when the quality of the work performed is checked and a site is inspected where no renovation work has been carried out. In

the thermography images, one can make sure that an uninsulated building has very large heat losses through external walls, old wooden windows, and window openings. According to the temperature scale in the thermography images, it can be seen that the building on the left has been renovated, exterior wall and loggia walls have been insulated. In the building on the right, there are visible heat losses both through the external walls and the window openings. The largest heat losses are observed in the joints of panels, window and door openings. Therefore, in the process of building renovation, it is important to pay attention to the quality of work, which is directly related to the joints of the building envelope, pretreatment of joints, anti-corrosion treatment of reinforcement, use of waterproofing mastic as well as insulation of windows and doorways, in order to reduce cold bridges.

During inspections, it is often found that if the project does not provide for the transfer of gas inlets and electrical cabinets from the building facade, large heat losses are observed through parts of the building that are not insulated, where insulation material offset is formed, because these gas inlets or electrical cabinets are not allowed to be completely "insulated". Also in the photo fixation attached to the tables one can see the location of these problems, in the gas inlet that is not insulated, there is increased heat loss, the surface temperature is higher than it would be if the facade surface were completely insulated.

Figures 6 and 7 below summarise the images of insulated and uninsulated multi-apartment residential buildings. It is possible to clearly see both thermography and photo fixation in the images.

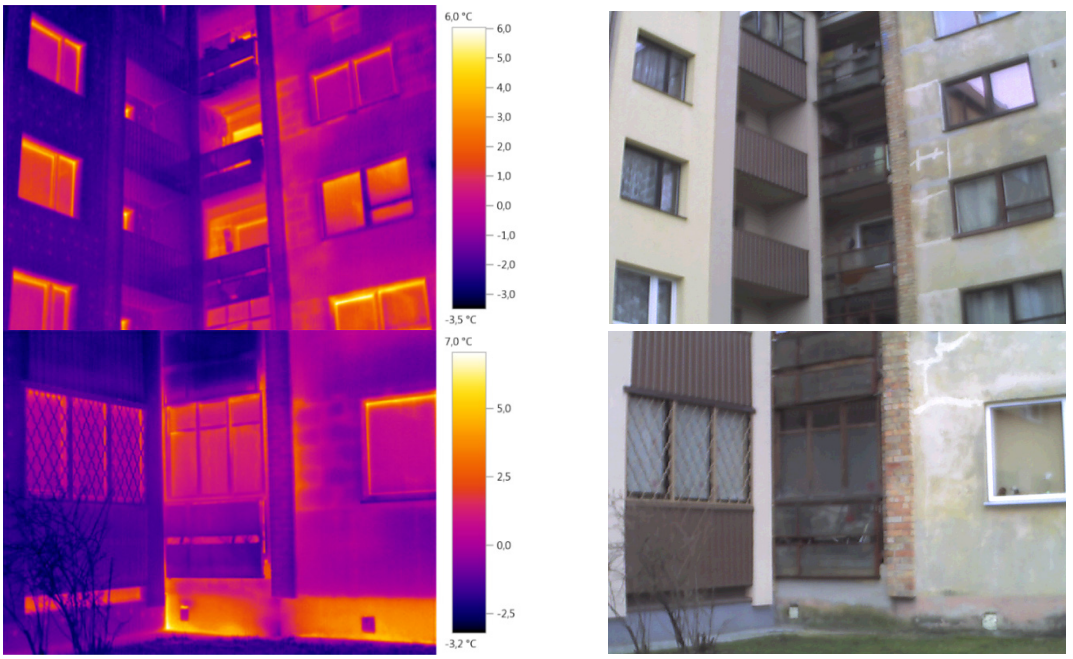

Fig. 6. Fixation from the work process (from the authors' archive).

In the "uninsulated building" (see Figs. 6 and 7), the thermal chamber shows very serious heat losses.

Uninsulated building

Insulated building

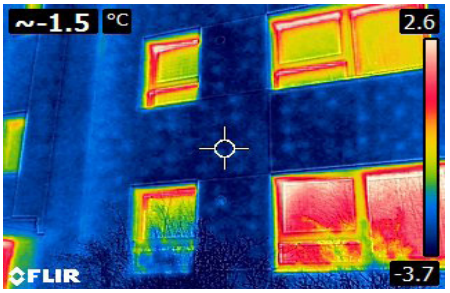

The left corner of the photo shows the temperature (C°) where the target is fixed (in the center of the photo). It is fixed to the plinth of the building. The problem is in the plinth part of the building; the surface is heated to +7.6 C°, which means that the basement has an increased temperature, the enclosing structure has low heat resistance and heat energy escapes when the plinth of the building is heated.

The photo shows that the insulated exterior wall has a high heat resistance; the high quality work has been performed. Questions could be asked here about the fastenings (dowels) of the thermal insulation material, as it can be observed they emit heat from the building structure.

Uninsulated building

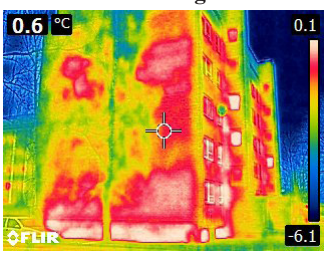

Insulated building

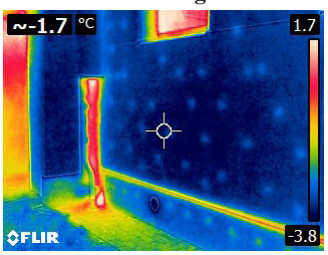

Insulated and uninsulated building

Uninsulated building

Insulated building

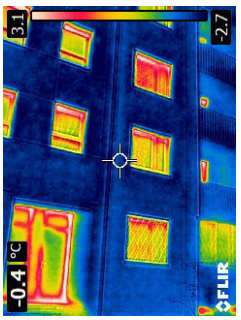

Insulated building

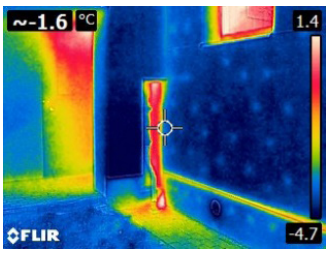

Fig. 7. Thermographs from building inspection (from the authors' archive).

Thermographic photographs show the intensity of heat loss through the enclosing structures of the building. The surface temperature can be compared to the outdoor air temperature. The closer the surface temperature is to the outdoor temperature, the better heat resistance properties of the surface (enclosing structure). Colour differences can also be accurately observed; the darker shade of blue colour, the better heat

resistance values the construction has due to less heat permeation through the parts of the building, lower heat loss.

It should be noted that measures affecting one system or part of a building may affect the energy performance of another system and part of a building. For example, the insulation layer of the enclosing structure affects the capacity and dimensions of the engineering systems. This interaction between different activities is taken into account when determining a complex solution for the renovation of a building.

Therefore, in DME projects, the authors observe that building renovation measures are combined into a set of measures and options, because meaningful combinations of measures can create synergies, providing better results (in terms of cost and energy efficiency) than individual measures. If more cost-effective energy efficiency measures are included in the set of measures, this may provide an opportunity to include other measures that are not cost-effective but can significantly increase primary energy use and reduce CO_2 emissions in relation to the overall building concept, provided, however, that the whole set of measures brings greater benefits than costs during the operation of the building or building elements. In turn, when implementing complex energy efficiency measures, it is also possible to improve the aesthetic parts of the building (staircases, porches, etc.).

4. CONCLUSIONS

To achieve the best possible result, it is necessary to develop the building renovation project in as much detail as possible, as well as to choose thermal insulation and finishing (plastered and ventilated facade) solutions, evaluating economic and technological aspects.

In the case of complex renovation of a building, the achieved energy savings, if both design and construction conditions are observed during the project implementation, shall be not less than 50 % of the previous consumption.

The authors conclude that the current costs and the deadline for the preparation of technical documentation are not commensurate with the quality of the developed works. Most multi-apartment buildings are constructed according to standardised designs, so the design should be simpler, but with a comparatively finer approach to technical solutions, where attention should be paid to detail and the total investment costs should be calculated according to the energy saved.

Achieving a high-quality, cost-effective and energy-efficient result is based on the development of a standardised building renovation project with a detailed description of the economy and achievable energy efficiency indicators, which is explained to homeowners in order to better and more effectively meet owners' needs, reach lower utility costs and achieve energy efficiency indicators.

ACKNOWLEDGEMENTS

The research has been supported by the project of the National Research Programme "Trends, Challenges and Solutions of Latvian Gas Infrastructure Development" (LAGAS) (No. VPP-EM-INFRA-2018/1-0003).

REFERENCES

1. Amanaditis, G. (2020). *Combating climate change.* Available at https://www.europarl.europa.eu/factsheets/lv/sheet/72/cina-pret-klimata-parmainam
2. *Ēku energoefektīvas renovācijas koncepcija Juglai*. (2010.) SIA Pilsētmāju pārvaldnieks. Available at http://www.rea.riga.lv/files/urbenergy/Eku_energoefektivas_renovacijas_koncepcija_Juglai_1dala.pdf
3. Savickis, J., Zemite, L., Bode, I., & Jansons, L. (2020). Natural Gas Metering and its Accuracy in the Smart Gas Supply Systems. *Latvian Journal of Physics and Technical Sciences, 57* (5), 39–50. DOI: 10.2478/lpts-2020-0026
4. Nieboer, N., Gruis, V., Van Hal, A., & Tsenkova, S. (2011). Energy efficiency in housing management – Conclusions from an international study. In *ENHR Conference*, 5–8 July 2011. Available at https://www.academia.edu/1782670/Energy_efficiency_in_housing_management_conclusions_from_an_international_study
5. Directive 2012/27/EU of the European Parliament and of the Council on energy efficiency, amending Directives 2009/125/EC and 2010/30/EU and repealing Directives 2004/8/EC and 2006/32/EC, 25.10.2012. *Official Journal of the European Union.* 14.11.2012. Available at https://eur-lex.europa.eu/legal-content/EN/TXT/?uri=celex%3A32012L0027
6. Directive 2010/31/EU of the European Parliament and of the Council of 19 May 2010 on the energy performance of buildings. *Official Journal of the European Union.* 18.06.2010. Available at https://eur-lex.europa.eu/legal-content/en/TXT/?uri=CELEX%3A32010L0031
7. Ministry of Economics of the Republic of Latvia. (2018). *Ēku energoefektivitāte*. Available at https://www.em.gov.lv/lv/nozares_politika/majokli/eku_energoefektivitate/
8. Jasevičs, A., Zemīte, L., Gorobecs, M., & Klavina-Makrecka, S. (2019). The impact of season-dictated daylight saving measures on electricity consumption. In *IEEE 60th Annual International Scientific Conference on Power and Electrical Engineering of Riga Technical University, RTUCON 2019 – Proceedings.* Article number 8982303. 7–9 October 2019, Riga, Latvia.
9. Jasevičs, A., Zemīte, L., & Kuņickis, M. (2017). Demand load control with smart meters. In *58th Annual International Scientific Conference on Power and Electrical Engineering of Riga Technical University, RTUCON 2017 – Proceedings,* Vol. 2017-November (pp. 1–6). DOI: 10.1109/RTUCON.2017.8124757
10. Borodiņecs, A., Geikins, A., & Prozuments, A. (2020). Energy consumption and retrofitting potential of latvian unclassified buildings. *Sustainability in Energy and Buildings: Proceedings of SEB 2019. Smart Innovation, Systems and Technologies. Vol.163* (pp.319–326). Hungary, Budapest, 4–5 July 2019. Singapore: Springer Nature Singapore Pte Ltd., 2020, DOI:10.1007/978-981-32-9868-2_27
11. Pļaviņa, B., & Actiņa, G. (2020). Implementation of Energy Efficiency Management System in Multi-Storey Residential Houses in Littoral Regions of Latvia. *Baltic Journal of Real Estate Economics and Construction Management, 8* (1), 1–11. DOI: 10.2478/bjreecm-2020-0001
12. Hernandez, P., Burke, K., & Owen Lewis, J. (2008). Development of Energy Performance Benchmarks and Building Energy Ratings for Non-Domestic Buildings: An Example for Irish Primary Schools. *Energy and Buildings, 40* (3), 249–254. https://doi.org/10.1016/j.enbuild.2007.02.020
13. Martinaitis, V., Rogoža, A., & Bikmanien I. (2004). Criterion to Evaluate the "Twofold Benefit" of the Renovation of Buildings and their Elements. *Energy and Buildings, 36* (1), 3–8. https://doi.org/10.1016/S0378-7788(03)00054-9

14. Central Statistical Bureau. (n.d.). *Multi-Apartment Residential Buildings in Latvia.* Available at http://data1.csb.gov.lv/pxweb/lv/rupnbuvn/rupnbuvn__nek_ip/?tablelist=true. 2020
15. Altum: Development Finance Institution. (2020). *The Programme for Improving Energy Efficiency in Multi-Apartment Residential Buildings.* Available at https://www.altum.lv/en/services/energy-efficiency/energy-efficiency-in-multi-apartment-buildings/about-the-programme/
16. Ministry of Economics of the Republic of Latvia. (2014–2019). *Vidējais apkures patēriņš ēkās.* Available at https://www.em.gov.lv/lv/nozares_politika/majokli/petijumi__statistika/videjais_apkures_paterins_ekas_uz_01_03_2014_/

sciendo

LATVIAN JOURNAL OF PHYSICS
AND TECHNICAL SCIENCES
2020, N 6

DOI: 10.2478/lpts-2020-0033

THE SELECTION OF BORON NITRIDE CIRCLES FOR GRINDING SAPONITE–TITANIUM COMPOSITES USING NON-PARAMETRIC METHOD

N.M. Huliieva*, D.O. Somov, V.V. Pasternak, L.M. Samchuk, T.I. Chetverzhuk

Lutsk National Technical University,
75 Lvivska Str., 43018 Lutsk, UKRAINE
*e-mail: n.huliieva@lntu.edu.ua

The issue of grinding saponite–titanium composites has not been considered in the machine building industry yet. The reason is that the chips are stuck on the working surfaces of abrasive tools made of silicon carbide and electrocorundum. This is due to the high adhesive activity at operating cutting temperatures between the composite and traditional abrasives.

The article aims at studying the grinding of saponite–titanium composites using abrasive tools in various cutting modes based on parametric and non-parametric statistical methods.

To solve this problem, high porous wheels (HPW) made of cubic boron nitride CBN30 with 100 % concentration on a bond V (K27), a pore-forming KF40, varied grains: B76, B126, B151 (ISO 6106:2013) – and hardness: M and O (ISO 525:2013) were used to grind saponite–titanium composites. Additionally, the Norton wheels from green silicon carbide with a normal porosity 39C (46; 60) K8 VK and with different grain size were tested. Norton wheels provide reduction of roughness height by 1.4–1.5 times in comparison with boron nitride HPW. These are recommended for the finishing grinding stage and HPW CBN30 – the preliminary to reduce the thermal effects on composites. By processing stability, the Norton wheels with grain 46 rank first, and among boron nitride HPW – CBN30 B76 100 OV K27–KF40.

Keywords: *Abrasive tools, composite, grinding, parametric and nonparametric methods, saponite–titanium.*

1. INTRODUCTION

Saponite–titanium composite is a promising material for mechanical engineering thanks to the well-designed manufacturing technology and relatively low cost [1]–[3]. It has unique physical and chemical properties and is one of the most difficult to pro-

cess composite. Its properties make the cutting process difficult even when compared to processing materials such as cast iron and stainless steel. However, if you plan machining step-by-step using the necessary knowledge in the field and the appropriate tools and equipment, there is a possibility for the grinding process [4]–[14].

The goal of the study is to grind saponite–titanium composites using abrasive tools in various cutting modes.

The main objectives of the study are to select optimal equipment and tools, to choose the required cutting modes and to develop grinding techniques.The object of the study is finishing and fine grinding operations.The subject of the study is the regularities of the formation of quality parameters in the process of mechanical processing of fine grinding.

According to the results of the studies, it is established that when grinding saponite–titanium blanks traditional abrasives based on silicon carbide are used. This is due to the fact that saponite–titanium intensively gives electrons to aluminum atoms in corundum, causing adhesive wear of electrocorundum grains. Adhesion interaction with silicon carbide is less intense than with electrocorundum. The properties of the composite, which affect its interaction with abrasive materials, are reflected in their wear resistance. Thus, for saponite–titanium, the wear resistance of silicon carbide is twice as high relative to corundum materials [15]. Information on the choice of green silicon carbide grains is private and requires further study in each case. Abrasive materials whose atoms do not accept saponite–titanium electrons and thus minimize adhesion are cubic boron nitride (CBN) and diamond. Clogging of the working surface of the wheels is caused by the low antifriction parameters of the composite, which has low wear resistance and a high tendency to ignition during friction. The thin oxide film is easily destroyed because it is thinner than the inner material, due to the diffusion of hydrogen, oxygen and nitrogen at grinding temperatures, starting from 350 ... 550 ºC [16]–[18]. The surface quality of saponite–titanium parts is evaluated by the surface roughness, which is one of the most important parameters in topography. They are formed by the following primary values:

$$H=\sum_{m=1}^{5} h_m \sum_{m=1}^{5} h_m, \quad (1)$$

where $h_1 h_1$ is a component of the profile that reflects the kinematic transfer of the geometric characteristics of the relief of the working surface of the tool on the workpiece (mold); $h_2 h_2$ is a component that arises as a result of oscillations of the circle and the workpiece due to different heights and chaotic arrangements of grains in the bundle; $h_3 h_3$ is a component due to plastic deformation of the surface when cutting grains into the metal; $h_4 h_4$ is a component of the adhesive interaction of grains with the workpiece; $h_5 h_5$ is a component of elastic deformations of the circle.

According to authors [19], the dominant component is $h_1 h_1$, and all others h_m h_m, $h_m h_m = \overline{2; 52; 5}$ are secondary values. It is established that the radius of the cutting part of the grains depends not only on their material, but also on the depth of incision in the metal. As the depth increases, individual small scratches merge into large one [12]. The weakest link in the technological system of the grinding process is the abrasive circle. At the same time, in the considered publications the emphasis is put on other technological parameters and conditions of grinding, and circles apply without the

necessary substantiation. For this reason, it has been decided to dwell on the choice of grain size of CBN HPC and Norton circles of standard porosity, as well as to further study the effect of hardness of CBN HPC on surface roughness. Given the sensitivity of the saponite–titanium alloy to stress concentrators, we consider it appropriate to optimise the characteristics of the circles by the criterion of roughness of parts, taking into account the surface roughness.

2. MATERIALS AND METHODS

For the experiment, we used 3D711VF11, 3G71M flat-grinding machines [20] and abrasive circles for grinding. The shape, size and technological parameters are shown in Table 1.

Table 1. Basic Parameters of Grinding Circles

Circle	Shape and dimensions	Technological parameters				
		Speed, V_g, m/s	Traverse, S_t, m/min	Cross feed, S_c, mm/ double movement	Cutting depth, t, mm	Operating overmeasure, z, mm
HPC CBN	1A1 200×20×76×5	30	8	6	0.01	0.1
Norton	01 250×20×76	35				

During the experiment, S_c feed is selected for two passes, so it makes sense to explain the functional purpose. Lowering the table to the depth was performed when the longitudinal table was shifted to the leftmost position relative to the operator. In this regard, moving the table from left to right is considered working. Cutting of metal from the surface was carried out according to the counter-grinding scheme, since the circle had to rotate clockwise. Then the reverse movement of the table together with the workpiece within the specified feed of the S_c became opposite. Given that the value of the S_c is less than the height of the abrasive tool, the residual working surface of the circle provides processing of the surface of the longitudinal movement of the table in both directions. In this case, the finishing pass of the tool occurred in the conditions of passing grinding. The circle embedding scheme was chosen based on the results of research [19], in which saponite–titanium alloy billets were processed under deep (single-pass) grinding conditions and received a reduction in the roughness height by one categorical value (CV) [21] in comparison with the alternative counter-grinding scheme.

Samples of saponite–titanium were used for the experiment [1]. Their physical parameters are shown in Table 2. Grinding was performed on the plane N. Coolant 5 % emulsion Aquol 11 (TU 38.101932-83) was supplied by irrigation to the part with a flow rate of 8 ... 12 l/min.

Table 2. Physical Parameters of Experimental Samples

Composite	Size, D × h, mm	σ, MPa	δ, %	E, GPa
Saponite–titanium	3.5 × 50	700	6 ... 10	60

The number of duplicate experiments – n = 20; i = $\overline{1; 20}$. Variable grinding conditions are represented by the code "dijv", which is convenient for analysing the initial process parameters using statistical methods. In this case, the index d = 1; 2 shows the direction of the roughness arrangement: 1 is parallel to the vector S_c, 2 is parallel to the vector S_t. Circle characteristics are encoded by the index i = $\overline{1; 6}$: 1 is CBN30 B76 100 OV K27-KF40; 2 is CBN30 B126 100 MV K27-KF40; 3 is CBN30 B126 100 OV K27-KF40; 4 – CBN30 B151 100 OV K27-KF40; 5 is 39C 46 K8 VK; 6 – 39C 60 K8 VK. HPC i = $\overline{1; 4}$refer to cubic boron nitride (CBN) instruments [22], in which the grain size varies from B76 (200/250) to B203 (120/140) and hardness from M (average) to O (average hardness) [23]. Norton i = $\overline{5; 6}$ circles of green silicon carbide grains of the 8th structure (normal porosity) have a medium hardness (K) and differ in grain size: 46 (355 ... 300 μm) and 60 (300 ... 250μm) according to ISO 8486-1:1999 [24], where the basic fraction are given in parentheses. Index j = $\overline{1; 3}$ is used in the scattering coefficients: 1 is for SD_{di}; 2 is for R_{di}; 3 is for QL_{di}.

Surface roughness measurements were performed using a system based on a profilograph: profilometer model 252 of the plant "Caliber" [25]. The system is a contact device for sequential conversion of the profile type AI. The device is intended for measurement in laboratory languages of roughness and roughness of a surface of products from metal and nonmetallic products. Its technical characteristics are given in Table 3. The measurement is performed on a straight line of the cut plane.

Table 3. Technical Characteristics of the Profilograph: Profilometer Model 252

Parameters							Step compartment value, mm	Type of cutting agent	m, kg
profilograph		profilometer							
R_z, μm	l, mm	R_a, μm	H_{min}, H_{max}, μm	tp, %	n	l, mm			
0.02–250	50	0.02–100	0.1–100	0–100	up to 1000	1.5; 3; 6	0.08; 0.25; 0.8; 2.5	numbers	107.6

Profilograph: profilometer model 252 consists of a rack with a motor drive, a universal subject table, a control unit, a computing unit, a differential inductive measuring transducer with a diamond probe needle and a recording device.

During experimental studies, according to ISO 1302:2002 [21], the following parameters R_a, R_q, R_z, R_{max1} were determined related to the height properties of inequalities. R_a is the arithmetic mean deviation of the profile; R_q is the standard deviation of the profile; R_z is the height of the profile irregularities at ten points; R_{max} is the largest height of profile irregularities. Surface roughness has both technical and economic tasks. The main parameters are the requirements for accuracy, efficiency, reliability of parts and equipment of machines. They depend on many roughness parameters, mechanical characteristics of surface functionality and method of application. The main requirement is to improve the service life and performance of engineering products.

The arithmetic mean deviation of the profile R_a is the arithmetic mean of the absolute values of the deviations of the profile within the base length:

$$R_a = \frac{1}{l} \cdot \int_0^l |y(x)| \cdot dx, \quad (2)$$

where y is the deviation of the profile: the distance between any point of the profile and the center line, which is measured along the normal line drawn to the center

line through this point of the profile;

l is the base length.

The standard deviation of the profile R_q within the base length:

$$R_q = \sqrt{\frac{1}{l}\int_0^l y^2(x)dx}. \quad (3)$$

The height of the irregularities of the profile at ten points R_z is the sum of the average absolute values of the heights of the five largest protrusions of the profile and the depths of the five largest depressions of the profile within the base length:

$$R_z = \frac{\sum_{i=1}^{5}|y_{pi}| + \sum_{i=1}^{5}|y_{vi}|}{5}, \quad (4)$$

where y_{pi} is the height of the i largest protrusion of the profile;
y_{vi} is the depth of the i largest depression of the profile.

The maximum height of the irregularities of the profile R_{max} is the distance between the line of protrusions and the line of depressions of the profile within the base length.

In this paper, we consider the parameters of R_a, R_{max}, which are the most important for saponite–titanium composites, which primarily affect the quality and performance of manufactured parts.

Methods of statistical interpretation of experimental data. Taking into account the instability of the grinding process and the random formation of the roughness surface, the analysis of observations is carried out using statistical approaches. We consider them as random variables (RV) that form independent sets:

$$\{y_{iv}\} = \overline{1;6}, v = \overline{1;20}. \quad (5)$$

In technical applications, we use parametric and non-parametric statistical methods (for example, rank methods). Characteristics of one-dimensional frequency distribution for many (2) are [26]: where $\bar{y}_i = y_{i\bullet}$ for the first direction – the medium, SD_i – deviation standards, $R_i = |y_{max} - y_{min}|$ $|y_{max} - y_{min}|_i$ – scopes, $\tilde{y}_i$ – for the second direction – medians, $QL_{il} = |y_{0,75} - y_{0,25}|_i$ – quartile latitudes, covering 50 % of the majority of observations (2). The first frequency characterises the position measure (total value), the next – the scattering boundaries (precision). $A_{Si} = \left[\frac{3(y\cdot - \tilde{y})}{SD}\right]_i$ – shift irelative to yi• due to the asymmetry (curvature) of the distribution curves found from the expression.

Each method of statistics has its own area of rational application. For the parametric method, it is necessary that most of the values (2) satisfy the requirements of normality and homoscedasticity of the dispersion. The second restriction is that measurements (2) must be determined with high accuracy, because otherwise it may lead to the adoption of incorrect hypotheses. To check the obtained data, one must use a non-parametric method that is not related to the properties of random variables.

Performing a one-dimensional variance analysis (OVA) and multiple search for predicted values $(\bar{y}_{my\bullet})_i$, $i = \overline{1;6}$ is associated with large calculations, so we use the program Statistica 12 [27].

The technique of modelling fuzzy logic. Fuzzy logic is designed to create mathematical models based on linguistic reasoning, in which the language and experience of experts play a fundamental role. In this sense, fuzzy logic is equivalent to the theory of fuzzy sets, i.e., classes with inaccurate, blurred boundaries. The theory of fuzzy sets [28] is a generalization and rethinking of the most important areas of classical mathematics. Moreover, by fuzzy sets A_{il} we mean sets of ordered pairs composed of elements *yilv* of universal sets *{yilv}* and

the corresponding degrees of membership μ *{yilv}*:

$$A_{il}=\left\{\left(y_{ilv}, \mu_A(y_{ilv})\right);\ y_{ilv} \in \{y_{ilv}\}\right\}, \qquad (6)$$

where $\mu_A(y_{ilv})$ are characteristic functions indicating the degree to which *yilv* belongs to fuzzy sets A_{il}. When implementing the process of modeling fuzzy logic, attributes are created that are based simultaneously on measures of position and scattering, which is impossible for statistical methods.

3. EXPERIMENTAL RESULTS AND DISCUSSION

Data (2) were tested for uniformity of variances (null hypotheses H_0) for eight roughness parameters in two directions d= $\overline{1; 2}$ when working with circles i = $\overline{1; 6}$, for which three groups of criteria were used (w = $\overline{1; 3}$): 1 – Hartley, Cochran, Bartlett, 2 – Levene, 3 – Brown-Forsyth. According to the test results, H_0 was accepted if the majority of decisions in its favour were $f_0 \in [19]$. It is established that for roughnesses $(R_a, R_q, R_z, R_{max})_2$ in the longitudinal direction H_0 is accepted at $f_0 \in [29]$. In the orthogonal direction d = 1 for the first group of criteria w = 1, all H_0 are accepted with a minor error of the 2nd kind. According to other statistical indicators w = 2, 3, the homogeneity of variances was confirmed for the parameters R_{a1} (w =2; 3) and R_{q1} (w = 3) in the presence of an error of the 2nd kind. Hypotheses about the normality of data distributions (2) behind the circles i= $\overline{1; 6}$ and the roughness parameters are accepted by the Shapiro-Wilk criterion when performing inequalities: $\alpha_i > 0.5$. The test results are shown in Table 4.

Table 4. Normality of Data Distributions (2) for Circles i= ($\overline{1; 6}$) and Roughness Parameters

Circle i=$\overline{1;6}$							
		1	2	3	4	5	6
α_i, μm	R_{a1}	0.2986	0.2147	0.6014	0.2425	0.0916	0.7755
	R_{q1}	0.8765	0.4166	0.4241	0.1227	0.1137	0.8114
	R_{z1}	0.5735	0.8297	0.3391	0.0241	0.0982	0.9432
	R_{max1}	0.0009	0.8635	0.0047	0.0047	0.4036	0.3355
	R_{a2}	0.395	0.9493	0.047	0.1238	0.000002	0.000007
	R_{q2}	0.7233	0.6187	0.1249	0.1397	0.000001	0.000004
	R_{z2}	0.2472	0.9878	0.0112	0.0354	0.0002	0.00002
	R_{max2}	0.6004	0.7021	0.3524	0.2747	0.00001	0.00002

As can be seen from Table 4, the best results of the normality of the distributions were obtained by grinding the details of saponite–titanium nitriding HPC B126 with a hardness M (i = 2): from eight parameters H_0 we accept six. Given that the roughness parameters in the d = 1 direction exceed the longitudinal counterparts and prevail in ensuring the operational properties of the parts [21], the priorities between the circles should be redistributed. According to the indicators, the first position falls on the circle 39C (i = 6) with a grain size of 60, for which the normality of distributions throughout the transverse parameter is ensured. At the next position CBN HPC i = 1; 2. As we can see, the requirements for RV require that the parametric method is not fully met. There is a need to apply the priority direction of interpretation of exper-

imental data of rank statistics.

Evaluation of cutting properties circles under the provision of the move. At the first stage of the analysis of experimental data, we will clarify their relationship in two orthogonal directions. According to the experimental medians

$$\left(\frac{\tilde{y}_1}{\tilde{y}_2}\right)_i, \; i=\overline{1;6}, \tag{7}$$

it is established that for some roughness parameters, the ratios are:

$$\left(\frac{\tilde{R}_{a1}}{\tilde{R}a_2}\right)_i = 2{,}11 - 3{,}02, \tag{8}$$

$$\left(\frac{\tilde{R}_{q1}}{\tilde{R}q_2}\right)_i = 2{,}14 - 3{,}02, \tag{9}$$

$$\left(\frac{\tilde{R}_{z1}}{\tilde{R}z_2}\right)_i = 2{,}35 - 3{,}1, \tag{10}$$

$$\left(\frac{\tilde{R}_{max1}}{\tilde{R}_{max2}}\right)_i = 2{,}04 - 2{,}71. \tag{11}$$

The smallest anisotropy of the tool roughness is provided when grinding the nitroborne HPC CBN30 B126 100 MV K27-KF40, and the largest with a Norton grain size of 46 (i = 5). According to the roughness parameters, the smallest isotropy of the topography refers to R_z and the highest to R_{max}. Anisotropy of roughness d = 1; 2 should be used to enhance the performance of the parts, positioning them during grinding so that longitudinal roughness receives the highest load when operating the machines. When operating the machines, the greatest information (R_{a1}, R_{max1}) is located in the transverse direction.

The obtained experimental and expected maximum values will be analysed in two aspects: from the standpoint of statistics and grinding technology.

In the first case, it was found that for parameters R_a, R_q, R_z, R_{max1}, which were partially represented (Tables 5 and 6), twenty research medians $\tilde{y}_{li}$, i = $\overline{1;6}$ out of the total number N = 4 × 6 = 24 were smaller than the same research averages. However, for only one roughness R_{a12}, the parametric position measure exceeded the median by one RV. For the rest of the roughness range, the error $\tilde{y}_{li\bullet}$ relative to $\tilde{y}_{li}$ occurred within the RV. A situation, in which the median coefficients (5) were less than one, revealed additional reserves for improving machine performance or grinding performance. The results obtained indicate that it is advisable to use the rank method instead of the Gaussian method to the competitor, which "for other results" [29] showed less accuracy in searching for common values.

Table 5. Influence of Characteristics, Roughness Position and Coefficients (8)–(11) for Parameters R_{ali}

Circle i=$\overline{1;6}$							
		1	2	3	4	5	6
$y_{li\bullet}$	μm	2.862	2.969	2.989	2.676	1.663	1.792
$\tilde{y}_{li}$		2.735	2.981	2.866	2.639	1.643	1.734
$\bar{y}_{li}$		2.874	2.918	2.929	2.793	1.728	1.728
$\bar{y}_{mli}$		2.805	2.805	2.805	2.805	1.688	1.688
K_{mi1} (8)		0.944	1.002	0.947	0.974	0.976	0.956
K_{mi1} (9)		0.964	0.950	0.946	1.001	0.965	0.965
K_{li} (10)		1.000	1.070	1.036	0.953	0.591	0.624
K_{li} (11)		1.000	1.000	1.000	1.000	0.592	0.592

Table 6. Influence of Characteristics, Roughness Position and Coefficients (8)–(11) for Parameters R_{max1i}

Circle i=$\overline{1; 6}$							
		1	2	3	4	5	6
y_{1i}.	μm	2.862	2.969	2.989	2.676	1.663	1.792
$\tilde{y}_{1i}$		2.735	2.981	2.866	2.639	1.643	1.734
$\bar{y}_{1i}$		2.874	2.918	2.929	2.793	1.728	1.728
$\bar{y}_{m1i}$		2.805	2.805	2.805	2.805	1.688	1.688
K_{mi1} (8)		0.944	1.002	0.947	0.974	0.976	0.956
K_{mi1} (9)		0.964	0.950	0.946	1.001	0.965	0.965
K_{1i} (10)		1.000	1.070	1.036	0.953	0.591	0.624
K_{1i} (11)		1.000	1.000	1.000	1.000	0.592	0.592

Differences between the media coefficients (8) and (9) also confirm the need for the second stage of the OVA. The results are the same when evaluating the cutting properties of circles relative to formulas (10) and (11). The fact is that for the experienced medians (10), the cutting abilities of the circles i = $\overline{1; 4}$ differ from each other, and for the expected analogues $y_{mli} = \overline{2; 4}$ the coefficients are equal to one, including for the roughness $z_l(R_q, R_z)_{li}$. Thus, for boron nitride HPC i= 1; 4 grain varies from B76 to B151 and a decrease in the degree of hardness from O to M at 5 % level, which is considered insignificant. This is most likely due to the modulus of elasticity of saponite–titanium billets, which is almost one and a half times lower in comparison with steel. With an increase in the cutting temperature to 350 °C, it additionally decreases almost linearly [30], which increases the elasticity after the action of the composite, which leads to an increase in the cutting force on the inner surfaces of the grains. It strengthens the elastic tension in the technological link "blank-HPC", acting as a vibration damper [31]. These regularities are accompanied by a decrease in the components h_2 and h_5 in Eq. (5). Additionally, the elementary values of h_3 and h_4, respectively, are reduced due to the low plasticity of the saponite–titanium alloy and the high chemical inertness of CBN grains in relation to composite. However, h_3 we believe that when grinding, the cutting temperature is from 500 ... 600 °C or higher. This in turn can cause a significant reduction in strength and fluidity of saponite–titanium composites with improved ductility, as specified in [1] by continuous heating of samples and due to the fact that the temperature of the grinding surface is characterised by a high gradient of decrease. Additionally, the elementary values of h_3 i h_4, respectively, are reduced due to the low plasticity of the composite alloy and the high chemical inertness of CBN grains in relation to saponite–titanium.

According to the results of the research, the properties of grinding parts of saponite–titanium are most acceptable for the samples obtained under similar conditions for high-speed plates (HSP) B9Mo4Co8 and blanks made of steel 06Cr14Ni6Cu2MoWT. It was found that when grinding the HSP, the smoothest surface was provided for the B126 grain, which was less than two CV for B76 and B151. At the same time, the increase in the HPC hardness i = 2; 3 in the specified interval was accompanied by a decrease in the reference values by two CV. At the same time, when grinding 06Cr14Ni6Cu2MoWT blanks, the role of selecting the HPC hardness increased: the position boundaries for different roughness parameters decreased by 2 ... 3 CV. At the same time, the minimum roughness is reached at a grain size of B151. The results

obtained indicate that the modulus of elasticity of steel billets increases almost twice as compared to saponite–titanium ones. This increases the influence of CBN grain sizes and the hardness of CBN HPC on the formation of general roughness values. It was revealed that the recommendations for the choice of saponite–titanium, B9Mo4Co8, 06Cr14Ni6Cu2MoWT were different. As previously stated, the roughness (1) is affected by the value h1, and the rest are considered secondary values. However, the results of the studies showed significant differences in roughness at a constant component of h_1.

The cutting properties of Norton circles with a grit of 46 and 60 are provided for the expected medians of equivalence. Norton tools can reduce the roughness of CBN HPC by 1.5...1.54 times or by 3 CV. The results obtained allow concluding that it is advisable to perform rough grinding of the CBN HPC in order to minimise the thermal impact on the part [32] and finishing with Norton circles for effective reduction of micro irregularities.

When processing the batch of workpieces on the configured machines, the stability (reproducibility) of the process of grinding, which is regulated by scattering, plays a high role. Tables 7 and 8 present all three precision parameters (SD, R, QL)$_{1i}$.

In the case of non-parametric method, preference is given to the results predicted by QL_{1i} and coefficients (13). It was found that the variation of the granularity of the CBN HPC from B76 to B151 at a constant degree of hardness O was approximated by an extreme curve with a maximum of QL_{13} with grain B126. At the same time, the minimum dependence of the QL = ψ (graininess) for the parameters R_{a14}, R_{max14}, R_{q14} was reached when grinding coarse-grained HPC B151 (i = 4), and for the height of the irregularities of the profile – at grain B76 (i = 1).

For comparison, in the processing of blanks 06Cr14Ni6Cu2MoWT minimum QL is noted at the lowest grain size B76, and QL_{max} – at B126 for all roughness parameters. The latter figure completely coincided with the results of grinding of saponite–titanium parts. In the HPC i = 2; 3 only the degree of hardness varies from medium (i = 2) to non-solid medium (i = 3). The only correlation relationship with QL was not found between them: $QL_{12} = QL_{13}$ – for parameter R_{a1}; $QL_{12} < QL_{13}$ – for the highest profile height. Another situation was for the details of 06Cr14Ni6Cu2MoWT: the increase in the hardness of the HPC in the studied range caused a decrease in the scattering rate by parameters R_{a1} and R_{max1} by 2.5 and 2.3 times, respectively. The parametric precision estimates for the saponite–titanium parts are predicted to be more stable and positioned the HPC in the following increasing sequence of scattering measures: 1 – B76, 2 – B151, 3 – B126M, 4 – B126O. The minimum and maximum granularity precision for both methods of statistics coincided (see Tables 7 and 8).

Table 7. Selective Estimates of the Cutting Properties of Circles of Scattering Boundaries R_{a1i}

Circle i= $\overline{1;6}$							
		1	2	3	4	5	6
SD_{1i}	μm	0.041	0.057	0.068	0.050	0.040	0.038
R_{1i}		0.245	0.299	0.358	0.274	0.252	0.183
QW		0.048	0.078	0.078	0.052	0.043	0.075
K_{1ij}	j=1(12)	1.000	0.757	0.349	0.845	1.013	1.050
	j=2(13)	1.000	0.814	0.682	0.886	0.961	1.307
	j=3(14)	1.000	0.655	0.655	0.926	1.079	0.678

Table 8. Selective Estimates of the Cutting Properties of Circles of Scattering Boundaries R_{max1i}

Circle i= $\overline{1; 6}$							
		1	2	3	4	5	6
SD_{1i}	μm	0.282	0.396	0.622	0.322	0.261	0.268
R_{1i}		1.142	1.882	2.659	1.265	1.218	1.086
QW_{1i}		1.000	0.560	0.582	0.401	0.375	0.450
K_{1ij}	j=1(9)	1.000	0.712	0.451	0.868	0.892	1.029
	j=2(10)	1.000	0.597	0.420	0.892	0.924	1.039
	j=3(11)	1.000	0.740	0.712	1.029	1.099	0.919

For $(SD, R)_{1i}$, i = 2; 3 unambiguous results were obtained, indicating a decrease in the reproducibility of the grinding process with increasing the hardness of the HPC from M to O: 1.16 ... 1.56 times SD and 1.13 ... 1.41 times the magnitude. In both cases, the greatest reduction in the stability of the grinding process was provided for the parameter R_{max1}. As it was revealed before, at grinding of details of HPC observations (5) were characterised by a high degree of homogeneity of dispersions, and the rank method of their interpretation was chosen as a result of disturbances of normality of distributions (Table 1). Probably, for this reason, the results obtained are quite stable when evaluated by parametric scattering. It should be noted that increasing the stability of the grinding process by varying the hardness of the HPC must be carried out taking into account the material of the grinding parts. In particular, for saponite–titanium it is advisable to reduce, and for 06Cr14Ni6Cu2MoWT, on the contrary, to increase.

For Norton circles, the greatest stability is 1 QL_{1i}, i= 5; 6 and is shown when using larger grains 45. This characteristic was even higher than for the basic HPC i = 1, as evidenced by the coefficients (14): 1.079 ... 1.099. Parametric estimates of the scattering boundaries of Norton circles, especially on a scale, for most grinding cases showed an increase in the reproducibility of processing when using Norton circles with smaller grains (at a grain size of 60).

4. CONCLUSIONS

1. In terms of violations of homogeneity of variances and uniform distributions, a nonparametric method is widely used in technical applications. The Gaussian competitor turned out to be expedient, in particular, to search for event position. It has been established that the average medians decrease, although this phenomenon occurs within the framework of the CV. This is evidenced by the median coefficients (8) and (9), which are less than one, in most cases. This, in turn, allows increasing the grinding performance while maintaining the surface quality of the parts.

2. It has been found that when grinding parts made of saponite–titanium composite, Norton circles provide high quality surface treatment in comparison with the CBN HPC. According to the research results, the median coefficients differ by 1.4 ... 1.5 times. For this reason, the HPC CBN30 should be used for rough grinding to reduce the thermal impact of the circle on the part, and the Norton circle should be used for finishing grinding, where there are high requirements for the roughness of parts. Saponite–titanium composites have been found to be almost insensitive to variations

in the grain size and hardness of the circles. This is due to the low modulus of elasticity of the saponite–titanium alloy.

3. The dispersion range under variable grinding conditions is more variable compared to the median and average. When using CBN HPC, the smallest QL_{1i} is provided for i = 1; 4 (that is, for grains B76 and B151). For B126 grain, the stability of the QL_{13} process decreased by 1.2 ... 1.3 times. The variation in the HPC hardness from medium-hard (i = 3) to medium (i = 2) should be recognised as insignificant QL. Simultaneously, the $(SD\ R)_{1i}$ i = 2; 3 shows an increase in the precision of the process. Therefore, at a high level of uniformity of variances, parametric estimates are more accurate than quartile latitudes.

REFERENCES

1. Guliieva, N. M. (2015). *Getting Porous Penetrating Materials Using Natural Mineral − Saponite in Self-Propagating High-Temperature Synthesis*. − Manuscript. Dissertation for the degree of Ph.D., specialty 05.02.01 − Materials science. Lutsk National Technical University, 134.
2. Rud', V. D., Samchuk, L. M., & Gulieva, N. M. (2013). Using SHS process to obtain composite materials. *Powder Metallurgy: Surface Engineering, New Powder Composite Materials. Welding: Collection Doc*, 496–500.
3. Gulieva, N. M. (2014). Khimichnyi analiz ta fizychni vlastyvosti pryrodnogo material – saponitu. *Mizhvu zivskyi zbirnyk "Naukovi notatky"*, *44*, 78–82.
4. Kar, S., Kumar, A S., Bandyopadhyay, P. P., & Paul, S. (2020). Grindability of Plasma Sprayed Thermal Barrier Coating Using Super Abrasive Wheel. *Transactions of the Institute of Metal Finishing*, *98* (1), 30–36. DOI: 10.1080/00202967.2020.1697572.
5. Cao, J., Wu, Y., Li, J., & Zhang, Q. (2015). A Grinding Force Model for Ultrasonic Assisted Internal Grinding (UAIG) of SiC Ceramics. *Adv. Manuf. Technol.*, *81* (5–8), 875–885. DOI: 10.1007/s00170-015-7282-0.
6. El Wakil, S. D., & Srinagesh, K. (2008). Effect of the physical and mechanical properties of composites on their grinding characteristics. In *Conf. HPSM 2008*. April 2008 (pp. 149–155). WIT Transactions on the Built Environment 97: Grinding of polymeric composites. DOI: 10.2495/HPSM080161.
7. Bianchi, E. C., Rodriguez, R. L., Hildebrandt, R. A., Lopes, J. C., de Mello, H. J., da Silva, R. B., & de Aguiar, P. R. (2018). Plunge Cylindrical Grinding with the Minimum Quantity Lubrication Coolant Technique Assisted with Wheel Cleaning System. *Manuf Technol, 95*, 2907–2916. DOI: 10.1007/s00170-017-1396-5.
8. Wang, H., Ning, F., Hu, Yi., Fernando, P. K. S. C., Pei, Z. J., & Cong, W. (2002). Surface Grinding of Carbon Fiber – Reinforced Plastic Composites Using Rotary Ultrasonic Machining: Effects of Tool Variables. *Advances in Mechanical Engineering*, *8* (9). DOI: 10.1177/1687814016670284.
9. Irani, R. A., Bauer, R. J., & Warkentin, A. (2005). A Review of Cutting Fluid Application in the Grinding Process. *Int J Mach Tools Manuf*, *45* (15), 1696–1705. DOI:10.1016/j.ijmachtools.2005.03.006.
10. Miyakawa, O., Watanabe, K., Okawa, S., Nakano, S., Shiokawa, N., Kobayashi, M., & Tamura, H. (1990). Grinding of Titanium. 1. Commercial and Experimental Wheels Made of Silicon Carbide Abrasives. *Shika Zairyo Kikai*, *9* (1), 30–41. PMID: 2134811.
11. Jha, A., & Paul, S. (2019).Surface Integrity in Grinding of Ti-6Al-4V Using Monolayer Superabrasive Wheel. *Advances in Materials and Processing Technologies*, *5* (2), 213–225. DOI: 10.1080/2374068X.2018.1564866.
12. Das, P., Bandyopadhyay, P. P., & Paul., S. (2019). Finish Form Grinding of Thermally Sprayed Nano-Structured

Coatings. *Advances in Materials and Processing Technologies*, *5* (1), 39–52. DOI: 10.1080/2374068X.2018.1510680

13. Paul, S, Singh, A. K., &Ghosh, A. (2017). Grinding of Ti-6Al-4V under Small Quantity Cooling Lubrication Environment Using Alumina and MWCNT Nanofluids. *Materials and Manufacturing Processes*, *32* (6), 608–6015. DOI: 10.1080/10426914.2016.1257797
14. Li, H. N. (2016). Textured Grinding Wheels: A Review. *International Journal of Machine Tools and Manufacture*, *109*, 8–35. DOI: 10.1016/j.ijmachtools.2016.07.001
15. Kacalak, W., Lipiński, D., Bałasz, B., Rypina, Ł., Tandecka, K., & Szafraniec, F. (2018). Performance Evaluation of the Grinding Wheel with Aggregates of Grains in Grinding of Ti-6Al-4V Titanium Alloy. *Advanced Manufacturing Technology*, *94* (1–4), 301–314. DOI: 10.1007/s00170-017-0905-x
16. Kosmac, T., Oblak, C., Jevnikar, P., Funduk, N., & Marion, L. (1999). The Effect of Surface Grinding and Sandblasting on Flexural Strength and Reliability of Y-TZP Zirconia Ceramic. *Dental Materials*, *15* (6), 426–433. DOI: 10.1016/s0109-5641(99)00070-6
17. LópezdeLacalle, L. N., Rodríguez, A., Lamikiz, A., Celaya, A., & Alberdi, R. (2011). Five-Axis Machining and Burnishing of Complex Parts for the Improvement of Surface Roughness. *Materials and Manufacturing Processes*, *26* (8), 997–1003. DOI: 10.1080/10426914.2010.529589.
18. Niharika, Agrawal, B.P., Khan, I.A., & Khan, Z.A. (2016). Effects of Cutting Parameters on Quality of Surface Produced by Machining of Titanium Alloy and Their Optimization. *CC BY 4.0*, *63*, 531–548. DOI: 10.1515/meceng-2016-0030.
19. Soler, Ya. I., & Mai, D. S. (2015). Select of Abrasive Wheels while Pendular Grinding of Parts from Titanium Alloy VT22 by High Roughness Parameters. *Equipment. Tools, 4* (69), 18–33. DOI: 10.17212/1994-6309-2015-4-18-30
20. Catalog (2020). Metal cutting machines. *Catalog of metal-cutting machines and forging equipment.* Rubicon LLC. Available at http://stanki-katalog.ru/sprav.htm
21. ISO (2002). ISO 1302:2002, *Geometrical Product Specifications (GPS) – Indication of Surface Texture in Technical Product Documentation*.
22. ISO (2013). ISO 6106:2013, *Abrasive Products — Checking the Grain Size of Superabrasives*.
23. ISO (2013). ISO 525:2013, *Bonded Abrasive Products — General Requirements*.
24. ISO (1996). ISO 8486-1:1996, *Bonded Abrasives – Determination and Designation of Grain Size Distribution – Part 1. Macrogrits F4 to F220*.
25. ISO (1987). ISO GOST 19300-86. *Instruments for Measurement of Surface Roughness by the Profile Method. Contact Profilographs and Profilometers. Types and Main Parameters*. Available at http://docs.cntd.ru/document/1200004988.
26. Jiang, J., Roussas, G. G., & Samaniego, F. J. (2011). Nonparametric Statistical Methods and Related Topics. *World Scientific, 480*. DOI: 10.1142/8258.
27. Statistica: Enterprise Capabilities, *StatSoft*, 22. Available at http://statsoft.ru/#tab-STATIS
28. Ali, Y. M., & Zhang, L. C. (2004). A Fuzzy Model for Predicting Burns in Surface Grinding of Steel. *International Journal of Machine Tools and Manufacture*, *44*, 563–571.
29. Marinescu, I. D., Hitchiner, M. P., Uhlmann, E., Rowe, W. B., & Inasaki, I. (2006). *Handbook of machining with grinding wheels*. CRC Press. DOI: 10.1201/9781420017649.
30. Kikuchi, M. (2009). The Use of Cutting Temperature to Evaluate the Machinability of Titanium Alloys. *Acta Biomaterialia, 5* (2), 770–775. DOI: 10.1016/j.actbio.2008.08.016
31. Nik, M. G., Movahhedy, M. R., & Akbari, J. (2012). Ultrasonic-Assisted Grinding of Ti6Al4V Alloy. *Procedia CIRP*, *1*, 353–358. DOI: 10.1016/j.procir.2012.04.063.
32. ISO (2019). DSTU ISO 603-3:2019. *Communication Abrasives. Dimensions. Part 3. Internal grinding wheels. Amendment, 1*.

sciendo

LATVIAN JOURNAL OF PHYSICS
AND TECHNICAL SCIENCES
2020, N 6

DOI: 10.2478/lpts-2020-0034

EXHAUSTIVE STUDY OF THE PV MODULE IMPLEMENTED IN THE REGION OF ANNABA-ALGERIA

A. Dekhane[1*], B. Lamri[2], N. Benamira[2]

[1] The Higher School of Industrial Technologies – Annaba, ALGERIA
*e-mail: a.dekhane@esti-annaba.dz
[2] Badji Mokhtar – Annaba University, ALGERIA
e-mail: billel_la@hotmail.fr; nadir.benamira@gmail.com

Algeria, like any other country, has drawn up its roadmap for the use and promotion of renewable energy sources. Motivated by its commitment to the international community in the fight against global warming and its possession of one of the largest solar fields in the world, a series of laws and institutions have consolidated this ambitious schedule. As known, both the climate and the geological area of Algeria take place among the foremost favoured countries in the field of solar energy. The present paper aims at proposing a simple model of photovoltaic module.

The authors used Matlab/Simulink software to predict the current-voltage and power-voltage characteristics according to the influence of several factors, such as solar irradiance, cell temperature and series resistance, on the efficiency of photovoltaic module. The proposed experimental investigation can easily predict the curves (current-voltage and power-voltage) of a PV module, where both of simulation and practical results are identical. A single-crystalline photovoltaic module was introduced close to Badji-Mokhtar Annaba University, Annaba (Algeria) to show the impact of climatic conditions in this coastal region and partial shading on characteristics.

Keywords: *Algeria, photovoltaic module, series resistance effects, shading effects, simulation model, solar energy.*

1. INTRODUCTION

Nowadays, the development of renewable energy sources of all kinds, such as solar energy, wind energy, biomass energy etc., to produce electric energy has become more necessary than ever. The reason for this orientation is significant depletion of fossil

fuel stocks caused by increasing demand of manufacturers in developed countries. Furthermore, the emergence of natural disasters, due to global warming effect (the increased levels of carbon dioxide, chlorofluorocarbons, and other pollutants in the atmosphere), will affect the lives of future generations [1], [2]. All these factors have led scientists and researchers to study how to make good use of these renewable and environmentally friendly energy sources so that they can become alternative energy in the future.

Solar energy is one of the most important renewable energy sources due to its availability throughout the year and its presence almost everywhere. Solar energy represents a significant potential in Algeria because of its strategic geographic location.

According to the Centre for the Development of Renewable Energies in Algeria, average solar energy is estimated at 2,650 hours of sunshine per year in the north, and 3,000 hours in the highlands, 3,500 hours in the south of the desert. This allows Algeria to produce around 168.971 TWh of electricity per year, twice the capacity of Egypt and more than 100 times of Spain, which gives Algeria the preference to exploit this green energy [3].

There are two technologies for harnessing solar energy, the first being solar photovoltaic technology, which directly converts the sunlight into electricity through the use of semiconductor materials, such as silicon, that exhibit the photovoltaic effect [4]. The second is the solar thermal technology [5], which directly converts solar radiation into thermal energy used to heat domestic water and generate electricity indirectly as in Concentrating Solar Power [4], [6].

A PV module is a set of PV cells connected together in series or series / parallel in order to increase the power delivered by the PV cell. To increase the power produced up to a few MW, it is sufficient to connect the PV modules to each other in series / parallel and form what is called a PV field.

A photovoltaic system is subject to several factors that affect its performance, such as sunlight, temperature, shading [7]–[9], degradation [10], [11], [7], dust and dirt etc.

Studying the characteristics of PV modules is the most practical method for evaluating the performance of PV systems. Several researchers work in this field and have developed simulation models that simulate a PV module—PV field and give equations to calculate the parameters of these models [12]–[15]. However, an experimental study is needed to confirm the effectiveness of the simulation model especially for the east of Algeria like Annaba's region, which was never taken into consideration for such an exploratory study.

An experimental study has been carried out using a PV module Solo Line 80 model, which presented the effects of climate conditions in 'SIDI AMAR', Annaba city (Algeria), on its characteristics (I-V and P-V).

We propose a simple model of this PV module, using Matlab/Simulink Software, to calculate the PV module parameters of single-diode model and to predict its current-voltage and power-voltage curves according to the influence of several factors. We used in this model the input parameters provided by manufacturer's datasheet under Standard Test Conditions (STC) (G =1000 W/m^2 and T= 25 °C) such as Isc, Voc, ki, Ns, Imp, Vmp, kv. The curves of current-voltage and power-voltage of the PV module obtained experimentally illustrate the impact of partial shading on the PV module performance.

2. THEORETICAL STUDY

A. Photovoltaic Module Modelling

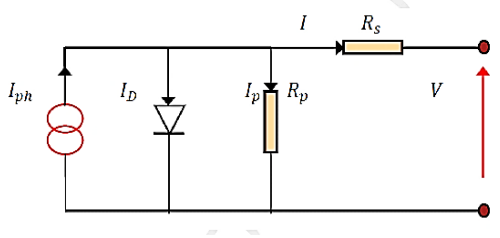

Fig. 1. Equivalent electrical circuit of photovoltaic module.

The electrical circuit of photovoltaic module based on the single-diode model [12, 15] is shown in Fig. 1, and described in Eq. (1).

$$I = I_{ph} - I_0 \cdot \left[exp\left(\frac{V+I.Rs}{a.Vt}\right) - 1\right] - \left(\frac{V+I.Rs}{Rp}\right), \quad (1)$$

where
I is the output current of PV module (A);
I_{ph} is the photovoltaic current (A);
I_0 is the saturation current of diode;
V is the output voltage of PV module;
Vt is the thermal voltage;
a is the diode ideality factor;
R_S and R_p are series resistance and shunt resistance, respectively.

The photovoltaic current mainly depends on the radiation intensity and cell operating temperature as follows [13], [16]:

$$I_{ph} = [I_{sc} + k_i * (T - T_{ref})] * \frac{S}{S_{ref}}, \quad (2)$$

where
I_{sc} is the short-circuit current (*A*);
k_i is the short-circuit current coefficient (*A/°C*);
T is the temperature of the p-n junction solar cell in *K*;
S is the solar radiation (*W /m²*);
S_{ref} is solar radiation at standard test conditions STC (25 °C, 1000 *W/m²*);
T_{ref} is the temperature at standard test conditions STC (25 °*C*, 1000 *W/m²*).

The saturation current of PV module is expressed in the following equation [7]:

$$I_0 = I_{r0} * [(\frac{T}{T_{ref}})^3 * exp(\frac{q*E_g}{a*k} * (\frac{1}{T_{ref}} - \frac{1}{T}))], \quad (3)$$

where
I_{r0} is the reverse saturation current (*A*);
k is the Boltzmann constant (1.38*10–23 *J/K*);
q is the electron charge (1.6 *10–19 °*C*);
E_g=1.12, is the Silicon Gap Energy (*eV*).

Temperature is one of the metrological parameters that affects the performance and degradation of PV modules (especially those installed in desert areas) [9], [10]. Equation (4) describes the mathematical calculation of the temperature of PV cells under the effect of ambient temperature:

$$T_m = T_{amb} + \left(\frac{T_{NOCT} - T_{ref}}{S_{ref}}\right) * S, \quad (4)$$

where T_{amb} is the ambient temperature, and TNOCT is the nominal operating cell temperature (NOCT) for operating at open circuit with the following conditions: ambient temperature of 20°*C*, irradiance S = 0,8 *kW/m²*, air mass (AM 1.5) and wind speed less than 1 m/s [13].

3. EXPERIMENTAL SETUP

The experimental results of PV module characteristics are obtained through the experimental setup as shown in Fig. 2. The PV module is mounted at Sidi Amar, in Annaba (latitude: 36 ° 49'3.58 "North, longitude: 7 ° 43'4.55" East and altitude 34 m). The tools and measuring devices are a PV module Luxor Solo Line 80, solarimeter Voltcrraft PL-110SM, Fluke 59 MAX infrared thermometer, multimeters, rheostat, and connection wires.

Furthermore, the proposed simulation model of PV module is presented in Fig. 3, where the solar irradiance, module temperature, open-circuit voltage at STC, short-circuit current at STC, and the number of cells per module are the inputs of model, while its outputs are the current and power.

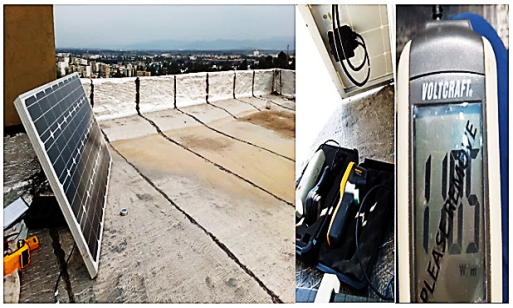

Fig. 2. Experimental setup and measurement devices.

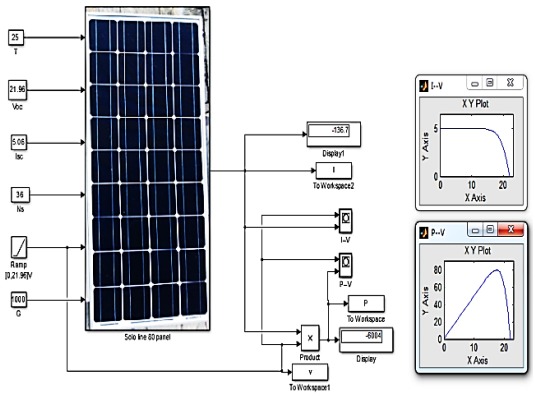

Fig. 3. Simulation model of a PV module.

Table 1 presents specific electrical parameters of PV module used in this study.

Table 1. Specification of the PV Module (Luxor Solo Line 80)

Parameters	Value
Maximum power (Pmp)	80 W (+/- 3 %)
Maximum power voltage (Vmp)	17.86 V
Maximum power current (Imp)	4.50 A
Open circuit voltage (Voc)	21.96 V
Short-circuit current (Isc)	5.06 A
Max system voltage	1000V
Number of cells per module (Ns)	36

4. RESULTS AND DISCUSSION

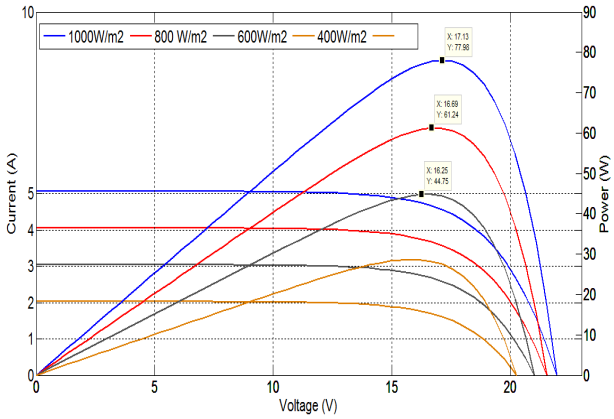

Fig. 4. (I-V& P-V) curves of PV module at different solar illumination values and constant temperature.

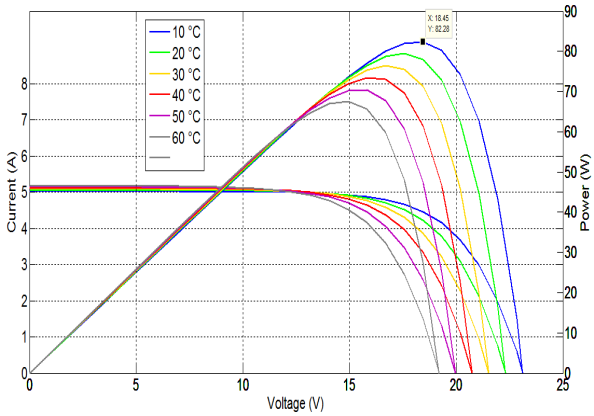

Fig. 5. (I-V& P-V) curves of PV module at different temperature values and constant solar illumination.

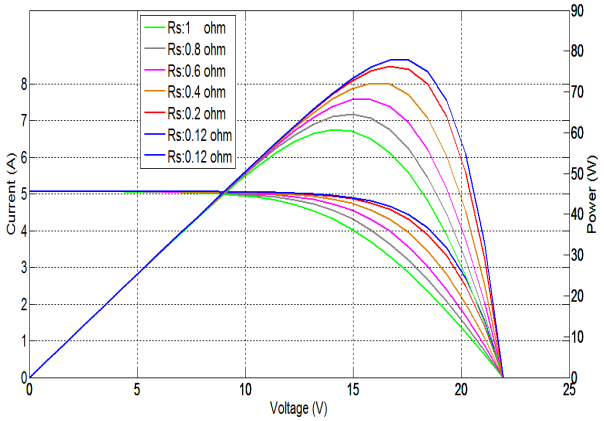

Fig. 6. Characteristic curves of PV module for different Rs values.

Figure 4 illustrates the current and power curves of PV module under different solar irradiance values (400 W/m^2 to 1000 W/m^2) obtained by simulation.

We observe from Fig. 4 that the increase in the solar irradiance value is accompanied by an increase in a short-circuit current value of PV module, which also leads to an increase in the maximum power value, and the opposite is true. While the increase in the solar irradiance value leads to a smaller increase in the open-circuit voltage value.

MATLAB simulation result of the purposed PV module in Fig. 5 shows I-V and P-V characteristics curves of PV module obtained under different values of PV module temperature (10 °C to 60 °C), and with constant solar irradiance value (1 KW/m^2).

We notice from both curves in Fig. 5 that the increase in the module temperature value leads to the decrease in the open-circuit voltage value, which results in a decrease in the maximum power point of PV module, while the short-circuit current value stays almost constant.

Figure 6 explains the effect of series resistance Rs on the I-V and P-V curves of PV module.

We notice that the increase in the series resistance values due to bad contacts, cell defect or other problems (degradation) [11] leads to a change in the form of curves from knee-shape to a straight-shape curve (Fig. 6) because of the decrease in the terminal voltage values of PV module. Thus, it leads to the decrease in the maximum power point.

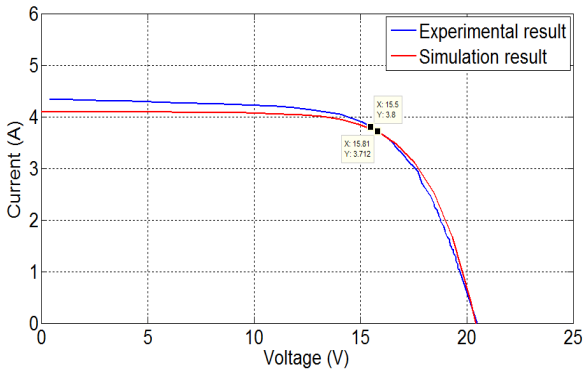

(a)

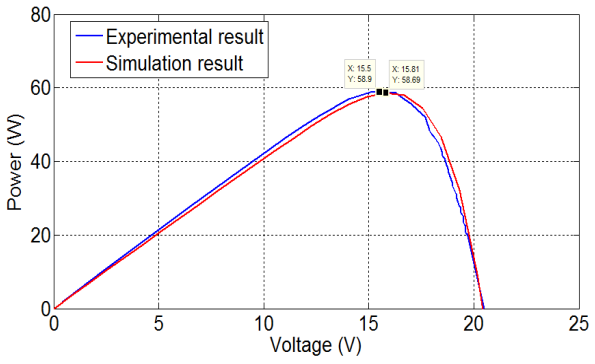

(b)

Fig. 7. Experimental and simulation, (a) I-V and (b) P-V characteristics of PV module.

Figure 7 (a, b) illustrates the current-voltage and power-voltage curves, respectively, of PV module taken under outside conditions (blue curves), while the simulation results are shown in the red curves.

We notice that the maximum power produced by the PV module was about 58.9 W on 14 April 2017 at 10.22 H (S= 820 W/m^2 and T = 44 °C) (see Fig. 10), corresponding to the maximum current and voltage (3.8 A, 15.5 V). Moreover, the results of simulation model and experimental measurements are identical, as shown by the red and blue curves in Fig. 7.

Figures 8 and 9 show the influence of shading on the characteristics of PV module. Figure 8 demonstrates the current-voltage and power-voltage curves of shading of PV module (PV half-cell), while Fig. 9 illustrates the influence of shading of a PV cell on the performance of PV module.

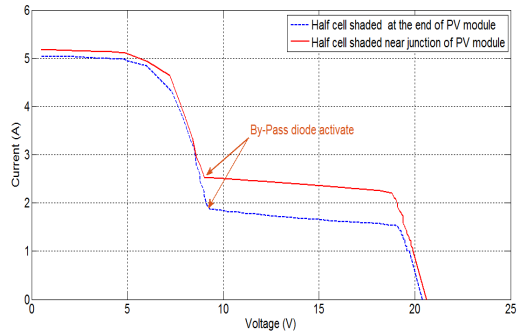

(a)

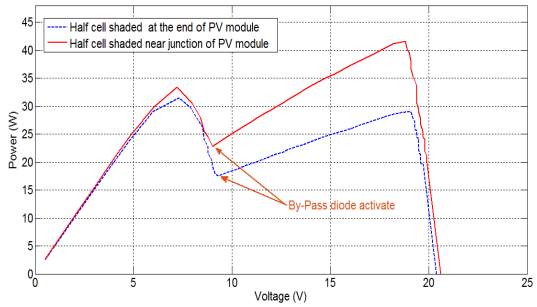

(b)

Fig. 8. Experimental (a) I-V and (b) P-V characteristics of PV module shaded half-cell at end, near junction.

In Fig. 8, we note that the shape of the current curve becomes a shape of two knees (Fig. 8 (a)) and two peaks in the power curve (Fig. 8 (b)) due to the inadequacy of the sunlight that reaches the shaded PV cell of the PV module (half PV cell). This leads to a reduction in the current and power of the PV module.

In Fig. 9, one observes an important division in the curve of the current and power due to the operation of the by-pass diode, which occupies the series of cells connected with the shaded PV cell, in order to protect them from hot-spot phenomenon. This leads to a significant decrease in power and PV module current.

We conclude from the experimental results (Figs. 8 and 9) that shading has a significant impact on the performance of the PV module.

Figure 10 presents the variation of solar illumination and the cell temperature values taken in the clear day, on 14 April 2017 in Sidi Amar, ANNABA. We can see that irradiance reaches the maximum value of 960 W/m^2 at 11:44 and decreases until sunset. Furthermore, the value of solar irradiance in this region can reach around 1100 W/m^2 in the middle of the day in April, indicated by solarimeter instrument (see Fig. 2). These values of solar irradiance and cell temperature according to daylight hours are shown in Fig. 10.

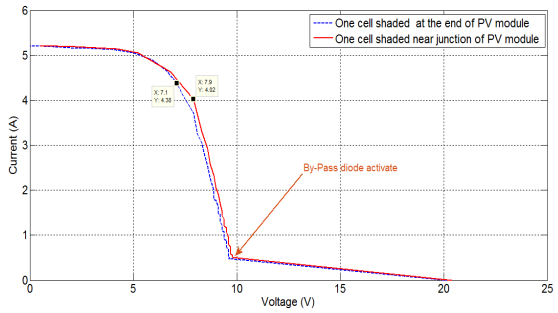

(a)

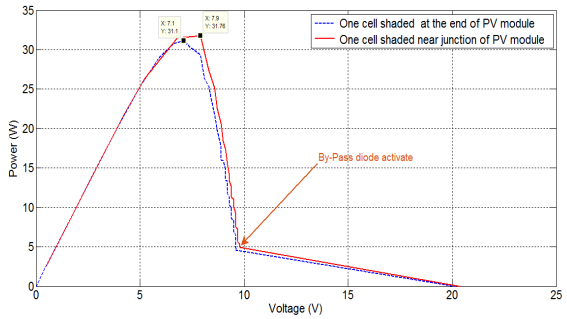

(b)

Fig. 9. Experimental (a) I-V and (b) P-V characteristics of PV module shaded one cell at end, near junction.

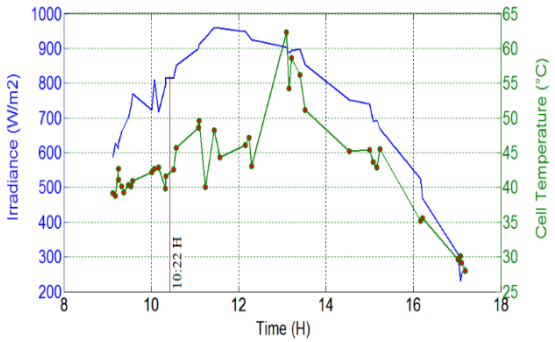

Fig. 10. Solar irradiance and cell temperature taken on a clear day.

CONCLUSION

From the research carried out, an experimental study has been presented. Its aim has been to show the influence of the climate of Sidi Amar, Annaba (Algeria), on the characteristics (I-V) and (P-V) of the PV module, Luxor Solo Line 80.

A simple simulation model has been presented to determine the parameters of any PV module, as well as to forecast its characteristics. From the outcome of our investigation, it is possible to conclude that the comparison seems to demonstrate that the experimental results and the simulation results are almost identical, which proves the credibility of this model.

Summing up the results, it can be concluded that the proposed strategy and involvement should therefore have wide application, and researchers can rely on this demonstration to explore PV module degradation for these particular regions of Algeria, which have never been taken into consideration in previous research.

Finally, we encourage the use of this important branch of renewable energy in the Annaba region in several domains: agriculture, autonomous electrical system, pumping with a direct and high socio-economic impact such as employment opportunities, engineering activity development and design, procurement and production capacities to reach an adequate industrial integration capacity. All things being equal, the economic impact of this purpose seems positive.

It could also be used to provide electricity to relatively undeveloped regions that are not connected to the national grid.

Based on the promising results presented in this paper, work on the remaining issues is ongoing and will be presented in future papers.

REFERENCES

1. Halkos, G.E., & Tsilika, K.D. (2017). Climate Change Effects and their Interactions: An Analysis Aiming at Policy Implications. *Economic Analysis and Policy, 53*, 140–146. DOI: 10.1016/j.eap.2017.01.005.
2. Prăvălie, R. (2018). Major Perturbations in the Earth's Forest Ecosystems. Possible Implications for Global Warming. *Earth-Science Reviews, 185*, 544–571. DOI: 10.1016/J.EARSCIREV.2018.06.010.
3. Jeffres, A., Grimditch, P., Taslima, R., & Pinson, T. (eds.). (2014). *The Report Algeria*. Oxford Business Group. Available at https://oxfordbusinessgroup.com/algeria-2014
4. Allina, G.P., & Burns, M.E. (2019). Harnessing the Sun to See Anew. *Neuron*, *102* (6), 1093–1095. DOI: 10.1016/j.neuron.2019.05.051
5. Hansen, K., & Mathiesen, B.V. (2018). Comprehensive Assessment of the Role and Potential for Solar Thermal in Future Energy Systems. *Solar Energy, 169*, 144–152. DOI: 10.1016/j.solener.2018.04.039.
6. Bader, R., & Lipiński, W. (2017). Solar Thermal Processing. *Advances in Concentrating Solar Thermal Research and Technology*, 403–459. ISBN 9780081005163.
7. Lamri, B., Abderrezak, A., Razem, H., & Kahoul, N. (2018). Shading and Diode Fault Effects on PV Array Performances. *Transactions on Electrical and Electronic Materials*, *19*, 75–83. DOI: 10.1007/s42341-018-0021-0.

8. Das, P., Mohapatra, A., & Nayak, B. (2017). Modeling and Characteristic Study of Solar Photovoltaic System under Partial Shading Condition. *Materials Today, 4* (14), 12586–12591. DOI: 10.1016/j.matpr.2017.10.066.
9. Lupangu, C. & Bansal, R. C. (2017). A Review of Technical Issues on the Development of Solar Photovoltaic Systems. *Renewable and Sustainable Energy Reviews*, *73*, 950–965. DOI: 10.1016/j.rser.2017.02.003.
10. Bouraiou A., Hamouda M., Chaker A., Mostefaouia, M., Lachtar, S., Sadok M., … & Issam, A. (2015). Analysis and Evaluation of the Impact of Climatic Conditions on the Photovoltaic Modules Performance in the Desert Environment. *Energy Conversion and Management*, *106*, 1345–1355. DOI: 10.1016/j.enconman.2015.10.073.
11. Bouraiou, A., Hamouda, M., Chaker, A., Lachtar, S., Neçaibia, A., Boutasseta, N., & Mostefaoui, M. (2017). Experimental Evaluation of the Performance and Degradation of Single Crystalline Silicon Photovoltaic Modules in the Saharan Environment. *Energy*, 1–28. DOI: 10.1016/j.energy.2017.05.056.
12. Askarzadeh, A., & Coelho, L. d. S. (2015). Determination of Photovoltaic Modules Parameters at Different Operating Conditions Using a Novel Bird Mating Optimizer Approach. *Energy Conversion and Management*, *89*, 608–614. DOI: 10.1016/j.enconman.2014.10.025.
13. El Achouby, H., Zaimi, M., Ibral, A., & Assaid, E.M. (2018). New Analytical Approach for Modelling Effects of Temperature and Irradiance on Physical Parameters of Photovoltaic Solar Module. *Energy Conversion and Management, 177*, 258–271. DOI: 10.1016/j.enconman.2018.09.054.
14. Polo, J., Martín-Chivelet, N., Alonso-García, M.C., Zitouni, H., Alonso-Abella, M., Sanz-Saiz, C., & Vela-Barrionuevo, N. (2019). Modeling I-V Curves of Photovoltaic Modules at Indoor and Outdoor Conditions by Using the Lambert Function. *Energy Conversion and Management, 195*, 1004–1011. DOI; 10.1016/j.enconman.2019.05.085.
15. Ma, T., Yang, H., & Lu, L. (2014). Development of a Model to Simulate the Performance Characteristics of Crystalline Silicon Photovoltaic Modules/Strings/Arrays. *Solar Energy*, *100*, 31–41. DOI; 10.1016/j.solener.2013.12.003.
16. Belhachat, F., & Larbes, C. (2015). Modeling, Analysis and Comparison of Solar Photovoltaic Array Configurations under Partial Shading Conditions. *Solar Energy*, *120*, 399–418. DOI: 10.1016/j.solener.2015.07.039.